ALMA MATER STUDIORUM · UNIVERSITÀ DI BOLOGNA

SCUOLA DI INGEGNERIA E ARCHITETTURA · CESENA

CORSO DI LAUREA MAGISTRALE IN INGEGNERIA ELETTRONICA E DELLE TELECOMUNICAZIONI PER L'ENERGIA

TITOLO DELL' ELABORATO

ELECTRICALLY TUNABLE PIEZOELECTRIC BIMORPH CANTILEVER FOR ENERGY HARVESTING

Tesi di Laurea Magistrale in

Elettronica Dei Sistemi Digitali

Relatore

Prof. Ing.
ALDO ROMANI

Correlatori

Dr. Ing.
LORETO MATEU

Dr. Ing.
HENRIK ZESSIN

Presentata da

DAVIDE FABBRI

I SESSIONE · II APPELLO
A.A. 2015/2016

This page intentionally left blank.

Keywords:

Energy harvesting
Bimorph cantilever
Resonance frequency
Electrical tuning
MPPT algorithm

This page intentionally left blank.

Ringraziamenti:

Lo svolgimento della tesi presso l'istituto Fraunhofer di Norimberga è stata per me un'esperienza di rilievo e motivo di crescita sia dal punto di vista tecnico sia personale. Per questo motivo i miei ringraziamenti vanno al Prof. Ing. Aldo Romani per il sostegno ricevuto e l'opportunità concessa.

Vorrei inoltre ringraziare i miei correlatori Dr.-Ing. Loreto Mateu e Dr.-Ing Henrik Zessin per avermi seguito nel lavoro di tesi condotto all'interno dell'istituto.

Un abbraccio e un sincero grazie va ai miei colleghi conosciuti durante la mia permanenza all'estero con i quali ho vissuto piacevoli momenti di lavoro, ma anche di svago.

Rigrazio gli amici del Bounty Rimini per avermi accompagnato in questi 5 anni insieme, nei quali ho collezionato tanti ricordi indelebili.

Infine, vorrei ringraziare la mia famiglia e i miei amici di sempre, che non mi hanno mai fatto mancare il loro affetto e sostegno, soppratutto nei momenti più difficili.

This page intentionally left blank.

Contents

Abstract **9**

Introduction **11**

1 Theoretical study **12**
1.1 General background 12
1.2 Tuning technique 15
1.3 Cantilever Beam 18
1.4 Resonance frequency of Bimorph Cantilever 19
1.5 PZN-5.5%PT vs PZT piezoelectric materials 26
1.6 Tuning ratio: Analytical study 28

2 Bimorph cantilever manufacturing **31**
2.1 Fabrication process 31
2.2 Harvester 34

3 Measurements with Electrodynamic shaker **36**
3.1 Test stand for measurements 36
3.2 Piezoelectric output power 39
3.3 Tuning ratio: experimental results 42

4 Electrical equivalent circuit **46**
4.1 General background 46
4.2 Test stand for measurements 51
4.3 Impedance measurements 54
4.4 Electrical parameters 60

5 Self-tuning piezoelectric vibration **62**
5.1 Test stand for tuning the resonance frequency 62
5.2 Actuators and shunt capacitance 63
5.3 MPPT Algorithm: Perturb and Observe (P&O) 64
5.4 Results and considerations 68

6 Phase Shift approach **72**
6.1 Sinusoidal Excitation 72
6.2 Multisine excitation 79

7 Conclusion and future works **83**
List of figures 85

Abstract

Con la presente tesi viene esaminato un metodo per modificare la frequenza di risonanza di elementi piezoelettrici. Di fatto si basa sulla relazione esistente che c'è tra la rigidità di tali materiali e l'applicazione di un carico elettrico di tipo capacitivo ad essi accoppiato.

L'elaborato inizia con la presentazione dei cristalli utilizzati nel lavoro di tesi, concentrandosi sul processo di fabbricazione di un bimorph cantilever, impiegato come raccoglitore di energia, la cui frequenza di risonanza è facilmente modellabile mediante la legge di Newton e il modello di Euler-Bernoulli. Su tale struttura vengono condotte misure con shaker elettrodinamico e analizzatore d'impedenza ai fini di giustificare il modello analitico presentato.

Con lo scopo di sincronizzare la frequenza di risonanza del cantilever con la vibrazione dell'ambiente per ottenere la massima potenza immagazzinabile, viene proposto un algoritmo MPPT secondo l'approccio Perturba e Osserva (P & O), al quale è fornita in ingresso la tensione efficace di un layer di materiale piezoelettrico. Valutare la sua risposta in tensione, presenta dei limiti applicativi che hanno portato a prendere in considerazione un approccio totalmente differente, il quale si basa sullo sfasamento che c'è tra la tensione di un materiale piezoelettrico e il segnale di accelerazione impiegato come eccitazione.

Comparative e campagne di misure sono state condotte con l'obiettivo di avvalorare la bontà di quest'ultimo approccio, qualora si voglia sincronizzare la frequenza di risonanza dei piezo con segnali di vibrazione reali (treni, aerei ...) di dinamica variabile nel tempo sia in ampiezza sia in frequenza.

Introduction

Nowadays, the energy harvesting market has an important role in the electronic systems. The idea is to extend battery life or where it is possible to replace them by capturing enough energy to supply the whole system.

Energy harvesting is a process able to transform the environmental energy (mechanical, thermal ...) into ready to use electrical energy [1]. If we focus on harvesting mechanical vibrations, the piezoelectric actuators can be helpful in order to accomplish the above mentioned objective. Thus, a bimorph cantilever was built and used in transverse mode for evaluating its resonance frequency and tuning ratio. A piezoelectric element ensures a maximum output power when its resonance frequency is tuned with environmental vibrations, otherwise the output energy is very low. The real vibrations change within a certain bandwidth, for this reason it is very important to change the beam resonance frequency in order to have a wideband generator. Many solutions are proposed in literature to achieve this goal. However, in this thesis, an adjustable electrical load is used, it consists in placing different parallel shunt capacitance to an additional mechanically-connected piezoelectric element. The purpose is to change the stiffness of the resonator and also its resonance frequency. The objective is to make an automatic tuning of the resonance frequency by using the approach over described. A MPPT algorithm was developed in $MATLAB/Simulink^{®}$and compiled on dSPACE DS1104 controller board, in order to maximize the piezoelectric output power. The algorithm is based on Perturb and Observe ($P\&O$) technique which has the piezoelectric RMS voltage as input. Its limitations brought me to find another possible solution for following the vibration frequency, in particular the Phase Shift approach was investigated. It is based on the phase shift between the acceleration signal and the piezoelectric voltage, which gives us an important information for understanding when the resonance frequency is matched with vibration frequency.

The *first chapter* describes the Euler-Bernoulli beam theory used for modelling the bimorph cantilever. The piezoelectric materials used for this thesis are showed and evaluated in an analytical study in MATLAB, by introducing the technique for tuning the resonance frequency with the environment, in particular an electrical tuning.

The *second chapter* is focused on the bimorph cantilever fabrication process in order to make the impedance measurements collected in the *fourth chapter* where an electrical equivalent model of the piezoelectric material is obtained.

The *third chapter* shows the measurements done with an electrodynamic shaker for evaluating the tuning ratio experimentally. The MPPT algorithm implemented on Matlab/Simulink is described in fifth chapter, by using a sine wave excitation.

The *sixth chapter* wants to investigate the Phase shift approach e shows different measurements as a proof that this method works also for non-sinusoidal signals.

The *last chapter* reports my conclusions and future developments on this work.

Chapter 1

Theoretical study

1.1 General background

Piezoelectric elements are used to convert mechanical energy into electrical energy. The brothers Pierre and Jacques Curie were first to discover the piezoelectric effect [2] in 1880 and shown that certain materials exhibited electrical polarization when they were subjected to mechanical stress.

Piezoelectric elements belong to a group of materials known as ferroelectric. Ferroelectric have locally a random oriented electric dipoles when the elements are hated above their Curie temperature and an electric field is applied, the dipoles align themselves relative to the applied electric field, Fig. 1.1. In this manner, they keep the polarization when the material is cooled.

The piezoelectric ceramic behaviour can be explained with Fig. 1.2. By applyng a mechanical tension or compression to a previously poled piezoelectric material, the dipole moment associated changes and produces an electric field, and thus also a voltage. In particular, when a compression is given to the piezo along the direction of polarization, it generates a voltage with the same polarity respect the poling voltage. Instead, by keeping a tension along the direction of polarization, the piezoelectric element provides an opposite voltage respect the poling voltage. The poling direction is always assigned to the $3th$ direction. All other properties depends on it, and typically are expressed as x_{ij}, where i represented the charge direction and the second subscript (j) denotes the stress direction.

There are two main ways in which piezoelectric elements are used as energy harvesters:

- Longitudinal direction (mode 33);
- Transverse direction (mode 31), (mode 32).

The direction of applied stress is assigned relative to the poling direction. However, if the stress is in the same direction as the poling, it also is in the $3th$ direction and so on.

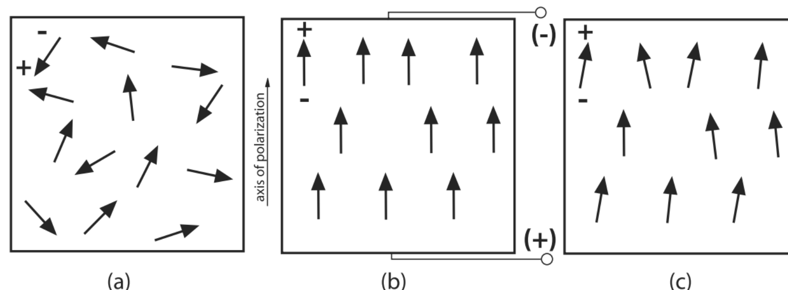

Figure 1.1: (a) Random oriented electric dipole before the polarization (b) During the polarization with a very large DC electric field. (c) After the process, the polarization is permanent.

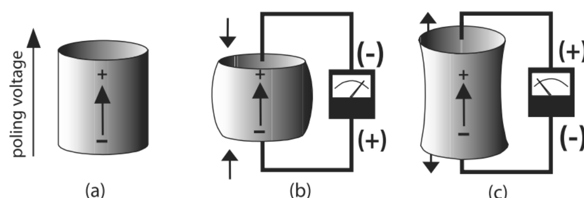

Figure 1.2: Piezoelectric behaviour

On each parameter of a piezoelectric element, these indexes have to be reported. Although, the 33 mode has higher converting coefficient than 31 mode, some advantages of 31 mode falling make the choice on it. In fact, the cantilever beam operating in the 31 mode is the best solution to provide the largest strain and generated power by keeping the same force as input, compared with the 33 mode, besides it is easier to reach a lower resonance frequency [3]. In my case, where is important to work with a low resonance frequency, a bimorph piezoelectric cantilever has been built and used in 31 transverse mode.

Before to see the details about it, for undesrtanding the piezoelectric mechanical behaviour is necessary to show the costitutive equations which describes the electromechanical properties for piezoelectric elements. As shown in *IEEE Standard on piezoelectricity* [4] this kind of materials are assumed to be linear. For this reason, both low electric field and low mechanical stress have a linear profile where the non-linear effects are negligible.

The equations, for the 31 mode, can be written in the following way:

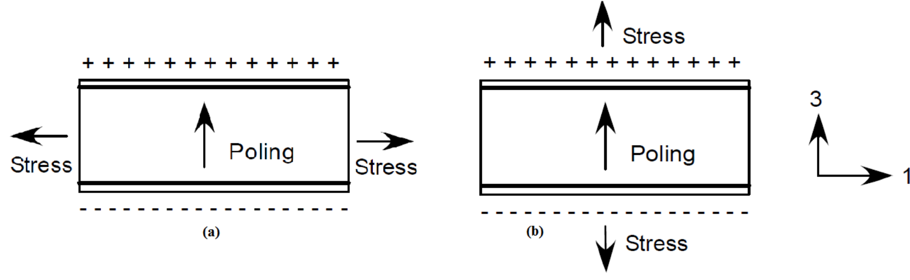

Figure 1.3: (a) 31 mode: charge harvested in third direction and stress applied in first direction. (b) 33 mode: both charge harvested and stress are applied in third direction.

$$S_1 = s_{11}^E T_1 + d_{31} E_3 \tag{1.1}$$

$$S_1 = s_{11}^D T_1 + \epsilon_{33}^T E_3 \tag{1.2}$$

$$D_3 = d_{31} T_1 + \epsilon_{33}^T E_3 \tag{1.3}$$

By combining (1.1) and (1.2):

$$s_{11}^E T_1 + d_{31} E_3 = d_{31} T_1 + \epsilon_{33}^T E_3 \tag{1.4}$$

$$s_{11}^D = s_{11}^E - \frac{g_{31} D_3}{T_1} + \frac{d_{31} E_3}{T_1} \tag{1.5}$$

By replacing (1.3) in (1.5):

$$s_{11}^D = s_{11}^E - \frac{d_{31}^2}{\epsilon_{33}^T} \tag{1.6}$$

- $\mathbf{s_{11}^D}$: Mechanical compliance of piezoelectric at open circuit conditions;
- $\mathbf{s_{11}^E}$: Mechanical compliance of piezoelectric at short circuit conditions;
- $\mathbf{d_{33}}$: Piezoelectric charge coefficient;
- $\mathbf{g_{31}}$: Piezoelectric voltage coefficient;
- $\epsilon_{\mathbf{33}}^{\mathbf{T}}$: Dielectric permittivity;
- $\mathbf{T_1}$: Mechanical stress (direction-1)

- $\mathbf{E_3}$: Electrical field (poled direction-3)
- $\mathbf{D_3}$: Electric flux density (poled direction-3)

A dynamic resonance frequency tuning is based on the dependence that exists between the mechanical stiffness and the electrical load to which it is subject.

As shown in (1.6), the deflection of the piezo can be modified in two different electrical load conditions:

- Open circuit (no charge displacement)
- Short circuit (zero electric field)

Under an applied mechanical force, in short circuit, the deflection of the material is higher (lower stiffness) rather than in open circuit.

We introduce another important parameter named *Electromecanical coupling factor* (k_{31}). It describes the ability of piezoceramic elements to convert electrical energy to mechanical one and vice versa.

$$k_{31}^2 = \frac{\text{Converted mechanical energy}}{\text{Input electrical energy}} = \frac{d_{31}^2}{s_{11}^E \epsilon_{33}^T} \tag{1.7}$$

$$\frac{d_{31}^2}{\epsilon_{33}^T} = k_{31}^2 s_{11}^E \Longrightarrow s_{11}^D = s_{11}^E - \frac{d_{31}^2}{\epsilon_{33}^T} = s_{11}^E(1 - k_{31}^2) \tag{1.8}$$

Piezoelectric materials with an higher electromechanical coupling coefficient permit to reach larger values of tuning ratio, by increasing the distance between both mechanical compliance at open circuit and short circuit conditions.

1.2 Tuning technique

Many solutions have been developed in order to match the piezoelectric resonance frequency with the external vibration for getting the maximum harvested power [5]. Hence, all of them are classified as function of the imput vibration signal:

- **Wide bandwidth vibrations:** the signal is smeared over a wide bandwidth with almost the same amplitude for all frequencies. For this reason, even if the resonance frequency is included in that bandwidth, the generator is not able to harvest the maximum energy.
- **Harmonic vibrations:** the signal is based on different harmonics where only one of them has the maximum peak. In this case, the tuning of the resonance frequency with the vibration is needed.

Fortunately, among the most common real vibrations, which come from trains, airplanes and so on, have a main harmonic in proximity of which most of the energy is distributed.

Thus, there are two different approches:

- **Active tuning of the resonance frequency:** the approach allows to adjust in real time the resonance frequency by using an active system. A power supply is required for making a dynamic tuning.
- **Passive tuning of the resonance frequency:** this method provides the possibility to tune the resonance frequency without any external device, which increases the power consumption of the system.

Although, the passive tuning does not steal any power supply from the piezoelectric material, because of the manual changing of the resonance frequency, it is not suitable for all those applications where it is required to autonomously tune the resonance frequency. For this reason, the active tuning was investigated in order to reach my objective.

In the literature [5] are shown different ways to make a dynamic tuning:

- **Application of an external force:**
  By applaying an external force in the same direction of the vibration, it induces a change on the mechanical stiffness of the piezoelectric generator besides of the resonance frequency. For example, the force could be generated from a magnetic field [6], by rotating magnets at a certain distance with the piezoelectric layers.
- **Application of an external DC electric field:**
  A DC electric field produces an effect on the piezoelectric stiffness as well [7]. Hence, by adjusting the amplitude of this field, the resonance frequency changes in controllable way. The literature shows that in order to have a big shift of the resonance frequency, a huge electric field is necessary. Then, it is not suitable for all those applications where the priority is to save the energy.
- **Adjustable electrical load:**
  The mechanical stiffness of piezoelectric materials can be moved in two different conditions: open circuit and short circuit, both explained in Section 1.1. However, by introducing an electrical load [5], the stiffness changes between the conditions over mentioned.

Many other solutions could be treated in order to achieve the goal of this thesis. Anyway, an adjustable electrical load has been chosen for moving the

piezoelectric resonance frequency, due to its simplicity and adaptability for making an autonomous system.

Now, It is important to find out which electrical load is fine, without decreasing the quality factor of the structure. For this reason, connecting different capacitors as non dissipative component represent the right choice.

The parallel capacitance connected to the piezoelectric element, called name *Shunt capacitance*. It is adjustable, in order to change the mechanical compliance between two extreme limits, as shown in (1.10) and the *Young's modulus* (Tab. 1.1). It is also known as elastic modulus and represents a mechanical propriety of a solid body that defines the relationship between *stress* (N/m^2) and *strain* (proportional deformation) applied on the material.

Eq. 1.8 shown in the previous section, can be written as follow:

$$C = C_p + C_s, \quad C_p = \epsilon_{33}^T \frac{A}{t_p} \tag{1.9}$$

$$s_{11}^D = s_{11}^E - \frac{d_{31}^2 A}{t_p(C_p + C_s)} \tag{1.10}$$

$$Yp = (s_{11}^D)^{-1} \quad \textit{Young's modulus} \tag{1.11}$$

Shunt Cond.	C_s	Z_{sh}	Y_p	**Stiffness**
Open C.	0	$(jwC_p)^{-1}$	$Y_{poc} = \left(s_{11}^E - \frac{d_{31}^2}{\epsilon_{33}^T}\right)^{-1}$	High Stiffness
Short C.	∞	0	$Y_{psc} = \left(s_{11}^E\right)^{-1}$	Low Stiffness
Cap. Shunt	C_s	$(jw(C_p + C_s))^{-1}$	$Y_p = \left(s_{11}^E - \frac{d_{31}^2 w_p L_p}{t_p(C_p + C_s)}\right)^{-1}$	Variable Stiffness

Table 1.1: Piezoelectric Young's modulus and stiffness as function of the Shunt capacitance.

where:

- $\mathbf{C_p}$: piezoelectric capacitance;
- $\mathbf{C_s}$: shunt capacitance;
- $\mathbf{t_p}$: piezoelectric thickness;
- $\mathbf{w_p}$: piezoelectric width;

- $\mathbf{L_p}$: piezoelectric length;
- $\mathbf{Y_p}$: Young's modulus.

1.3 Cantilever Beam

The Cantilever is a rigid structural element anchored at only one end to a support, from which it is protruding. In this thesis, only a fixed-free cantilever configuration is investigated, which can be built in two different ways [8]:

- Unimorph piezoelectric cantilever;
- Bimorph piezoelectric cantilever.

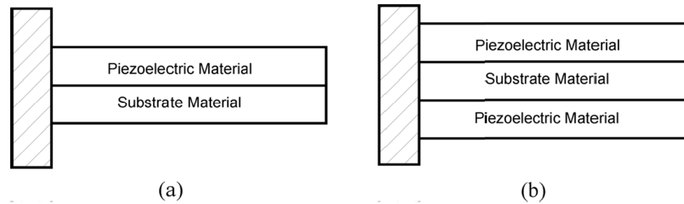

Figure 1.4: (a) Unimorph piezoelectric cantilever (b) Bimorph piezoelectric cantilever.

It is possible to see in Fig. 1.4, a *unimorph cantilever* is composed of a single piezoelectric element over a substrate. Instead, the other solution named *bimorph*, has two piezoelectric materials connected to the substrate. In both cases, a shim layer is present for adding mechanical stiffness to the structure as well as to make the device more durable.

In order to make a tunable generator, two piezoelectric layers are needed. The first one is used just for the output power, instead, the second one only for tuning the resonance frequency and changing the stiffness of the all structure. The operation of a cantilever bender is relatively simple, if a layer is in compression the other layer is in tension. It has a bidirectional behaviour and can be used like generator or actuator. The beam undergoes bending when an external force is applied (generator). This bending allows the charge accumulation between the electrodes of the piezoelectric layer. In the opposite case, when an electric field is applied to the piezoelectric layer, it expands or contracts and this causes the vibration (actuator).

In my work, the bimorph cantilever was treated as piezoelectric generator vibration-based.

1.4 Resonance frequency of Bimorph Cantilever

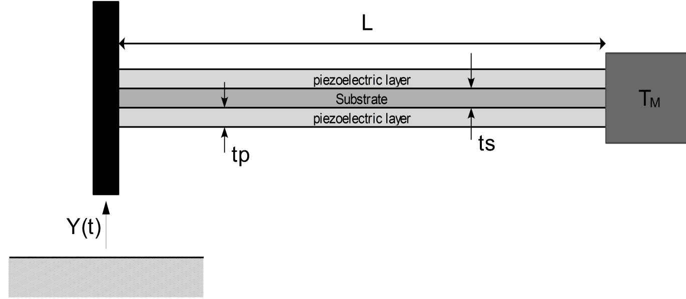

Figure 1.5: Bimorph piezoelectric cantilever.

In order to prove the relationship between the resonance frequency and the stiffness of the cantilever, Fig. 1.5 shows the model of bimorph cantilever (fixed-free) used for the mathematical formulation besides the construction of the beam [10].

Basically, it is based on a long slender beam of length L composed from two piezoelectric layers and one substrate of steel, with a tip mass (T_M) at the end.

The free-body diagram shown in Fig. 1.6 has been used for applying the *Newton's laws* [11]. It defines that in static equilibrium systems, where there is not motion, the sum of the forces and the moments in all directions must be zero respectively.

$$\sum forces = 0 \tag{1.12}$$

$$\sum moments = 0 \tag{1.13}$$

By applying (1.12) we get:

$$R - mg = 0 \quad \Rightarrow R = mg \tag{1.14}$$

At the left boundary (1.13):

$$M_R - mgL = 0 \quad \Rightarrow M_R = mgL \tag{1.15}$$

Hence, a segment of the Beam is shown in Fig. 1.7 by introducing a little deflection.

- **V**: Shear force
- **R**: reaction force
- **g**: gravitational acceleration

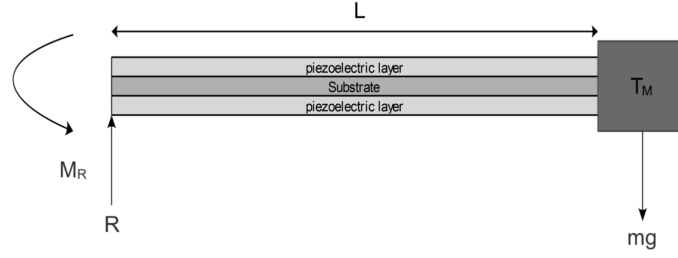

Figure 1.6: Free-Body diagram of the system.

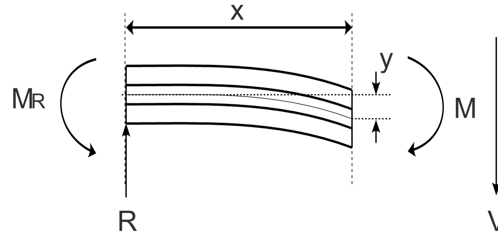

Figure 1.7: Segment of bimorph cantilever.

- **M**: Bending moment
- $\mathbf{M_R}$: reaction bending moment
- **m**: effective mass of the cantilever beam
- **y**: deflection of the neutral axis

By adding the moments at the right side of the segment:

$$M_R - Rx - M = 0 \quad \Rightarrow M = M_R - Rx \tag{1.16}$$

Jacob Bernoulli first discovered the relationship between the bending moment and the deflection of the neutral axis y, with a simplification of the linear theory [9]. For this reason, the model became the most commonly used for reasonable engineering approximations to solve many problems.

Now, by considering an infinitesimal segment of beam, he assumed that:

$$\epsilon_{xx} = \frac{dl}{l}; \quad \epsilon_{yy} = -\frac{dh}{h} \approx 0 \quad \Rightarrow \epsilon_{xx} >> \epsilon_{yy} \tag{1.17}$$

where:

- $\epsilon_{\mathbf{xx}}$: longitudinal strain (cause and effect are in x-direction)
- $\epsilon_{\mathbf{yy}}$: transverse strain (cause and effect are in y-direction)

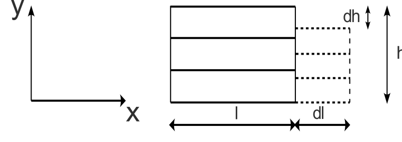

Figure 1.8: Infinitesimal part of the beam.

In Fig. 1.9 are shown two material fibres ab, pq of length Δx before and after a deformation, which deflection curve has a radius of curvature r. Nevertheless, the fiber pq has a distance u from the *neutral axis*, in this way, with the assumption $| ap |=| a'p' |$ and $| bp |= b'p' |$, the *longitudinal strain* is defined as:

$$\epsilon_{xx} = \frac{\Delta x' - \Delta x}{\Delta x} = \frac{(r-d)\Delta\theta - r\Delta\theta}{r\Delta\theta} = -\frac{u}{r} \tag{1.18}$$

The equation implies that with a small r (large curvature) the strain is bigger and vice versa. Furthermore, when $u > 0$ (over the neutral axis) the strain is always negative, instead, when $u < 0$ (below the neutral axis) the strain is positive.

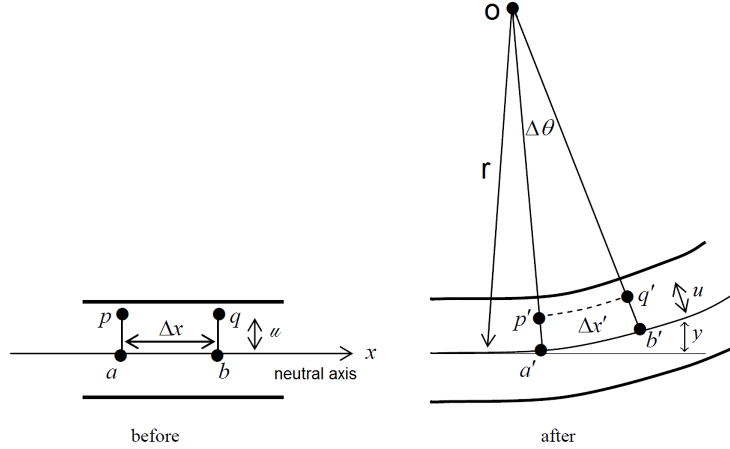

Figure 1.9: Deformation of the material before and after to apply a shear force.

At this point, in order to relate the deformation to the *stress*, the *Stress-Strain* relation from the *Hooke's law* [12] is needed:

$$\sigma_{xx} = E\epsilon_{xx} \tag{1.19}$$

Where, E is the Young's module of the whole structure and σ_{xx} represents the *longitudinal stress* (also in this case σ_{yy} is negligible). By introducing the Young's modulus of the piezoelectric materials (Y_p) and substrate (Y_s), the law can be written as follow:

$$\sigma_{xx} = (2Y_p + Y_s)\epsilon_{xx} = -\frac{(2Y_p + Y_s)u}{r} \tag{1.20}$$

For each materials where the slope of the deflection is small, we assume that:

$$\frac{1}{r} = \frac{d^2y}{dx^2} \tag{1.21}$$

The resultant force of the normal stress distribution over the beam section, must be zero and the resultant moment of the distribution is M.

$$0 = \int_A \sigma_{xx}\, dA = -\frac{2Y_p}{r}\int_{A_p} u\, dA_p - \frac{Y_s}{r}\int_{A_s} u\, dA_s \tag{1.22}$$

$$M = -\int_A \sigma_{xx} u\, dA = \frac{2Y_p}{r}\int_{A_p} u^2\, dA_p + \frac{Y_s}{r}\int_{A_s} u^2\, dA_s \tag{1.23}$$

A minus sign appears when we have a positive moment and positive dispacement (u) that implies a compressive (negative) stress.

$$\int_A u\, dA = \textit{first moment of area} \tag{1.24}$$

$$\int_A u^2\, dA = \textit{second moment of area} \tag{1.25}$$

$$\Rightarrow M = \frac{2Y_p}{r} I_p + \frac{Y_s}{r} I_s = (2Y_p I_p + Y_s I_s)\frac{d^2y}{dx^2} \quad \textit{moment-curvature equation} \tag{1.26}$$

where:

- $\mathbf{I_p}$: second moment of area of the piezoelectric material
- $\mathbf{I_s}$: second moment of area of the substrate

By combining (1.26) with (1.16) and subsequent replacement of (1.14), (1.15):

$$(2Y_p I_p + Y_s I_s)\frac{d^2y}{dx^2} = M_R - R_x = mgL - mgx = mg(L - x) \tag{1.27}$$

$$\frac{d^2y}{dx^2} = \left[\frac{mg}{2Y_p I_p + Y_s I_s}\right](L - x) \tag{1.28}$$

with an integration in spatial domain:

$$\frac{dy}{dx} = \left[\frac{mg}{2Y_p I_p + Y_s I_s}\right]\left[Lx - \left(\frac{x^2}{2}\right)\right] + a \tag{1.29}$$

Another integration is done for getting the beam displacement:

$$y(x) = \left[\frac{mg}{2Y_pI_p + Y_sI_s}\right]\left[L\left(\frac{x^2}{2}\right) - \left(\frac{x^3}{6}\right)\right] + ax + b \tag{1.30}$$

where:

- **a**: first integration constant
- **b**: second integration constant

The integration constants are obtained by applying the boundary conditions at (1.29) and (1.30):

$$y(0) = 0 \quad \textit{zero displacement (left end)} \quad \Rightarrow b = 0 \tag{1.31}$$

$$y'(0) = 0 \quad \textit{zero slope} \quad \Rightarrow a = 0 \tag{1.32}$$

Thus, the final equation of the displacement at the right end is:

$$y(L) = \left[\frac{mg}{2Y_pI_p + Y_sI_s}\right]\left[L\left(\frac{L^2}{2}\right) - \left(\frac{L^3}{6}\right)\right] = \left[\frac{mgL^3}{3(2Y_pI_p + Y_sI_s)}\right] \tag{1.33}$$

Hooke's law is used for evaluating the stiffness (K) of the cantilever beam:

$$F = Ky \tag{1.34}$$

where:

- **F**: force applied on the cantilever
- **K**: stiffness of the cantilever beam
- **y**: displacement of the neutral axis

The force at the end of the beam is $F = mg$ without applying others additional stresses. And so, the stiffness is written as:

$$K = \frac{F}{y} = \frac{mg}{\dfrac{mgL^3}{3(2Y_pI_p + Y_sI_s)}} = \frac{3(2Y_pI_p + Y_sI_s)}{L^3} \tag{1.35}$$

A vibration harvester is commonly modeled by a seismic mass m connected to a vibration source by a spring and a mechanical damper b_m, as shown in Fig. 1.10.

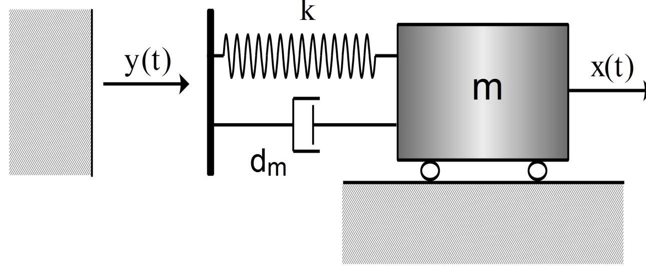

Figure 1.10: Equivalent mechanical model (SDOF).

It is a *single degree of freedom system* (SDOF) [13] that can be studied by applying the second *Newton's law* on the electromechanical model, which easily provides the angular frequency of the mass movement, given by:

$$\omega_n = \sqrt{\frac{K}{m}} \tag{1.36}$$

$$f_n = \frac{1}{2\pi}\sqrt{\frac{K}{m}} \tag{1.37}$$

The bimorph cantilever studied in my thesis is clamped from one side, where the vibration source is applied, while on the other side of the beam a tip mass is fixed and free to oscillate.

The *effective mass* (m) of the all structure is evaluated at the end of the cantilever and it is composed of both the beam mass (m_b), reduced by a multiplying factor, and the tip mass (T_M).

$$m = T_M + 0.24m_b \tag{1.38}$$

By replacing (1.38) and (1.35) in (1.37):

$$f_n = \frac{1}{2\pi}\sqrt{\frac{3(Y_{pT}I_p + Y_{pH}I_p + Y_sI_s)}{L^3(T_M + 0.24m_b)}} \tag{1.39}$$

where:

- $\mathbf{Y_{pT}}$: Young's modulus of the piezoelectric tuning layer, where the shunt capacitance is applied

- $\mathbf{Y_{pH}}$: Young's modulus of the piezoelectric harvesting layer
- $\mathbf{Y_{s}}$: Young's modulus of the steel layer used as substrate

The Young's modulus can be evaluated with a reference at Tab. 1.1 and each of them is rewritten in the following manner:

$$Y_{pT} = \left(s_{11}^{E} - \frac{d_{31}^{2} w_p L_p}{t_p (C_p + C_s)} \right)^{-1} \tag{1.40}$$

$$Y_{pH} = \left(s_{11}^{E} - \frac{d_{31}^{2} w_p L_p}{t_p C_p} \right)^{-1} \tag{1.41}$$

The *second moment of inertia* [14] is calculated by (1.25) for both cases: piezoelectric materials and steel layer, with the help of Fig. 1.11.

$$\begin{aligned} I_s &= \iint_{A_s} u^2 \, dA_s = \int_{-w_p/2}^{w_p/2} \int_{-t_s/2}^{t_s/2} u^2 \, dydx = w_p \left[\frac{u^3}{3} \right]_{-t_s/2}^{t_s/2} = \\ &= w_p \left[\frac{1}{3} \left(\frac{t_s}{2} \right)^3 + \frac{1}{3} \left(\frac{t_s}{2} \right)^3 \right] = \frac{w_p t_s^3}{12} \end{aligned} \tag{1.42}$$

$$\begin{aligned} I_p &= \iint_{A_p} u^2 \, dA_p = \int_{-w_p/2}^{w_p/2} \int_{t_s/2}^{t_s/2+t_p} u^2 \, dydx = w_p \left[\frac{u^3}{3} \right]_{t_s/2}^{t_s/2+t_p} = \\ &= w_p \left[\frac{1}{3} \left(\frac{t_s}{2} + t_p \right)^3 - \frac{1}{3} \left(\frac{t_s}{2} \right)^3 \right] = \frac{w_p t_p^3}{12} + w_p t_p \left(\frac{t_p + t_s}{2} \right)^2 \end{aligned} \tag{1.43}$$

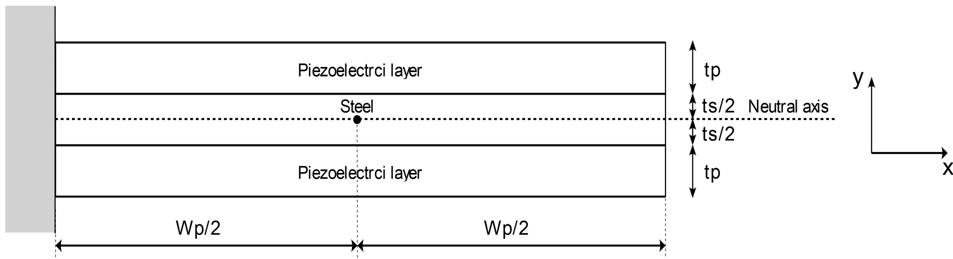

Figure 1.11: Bimorph cantilever.

Now, all the equations shown above can be replaced into the expression of the natural frequency (1.39). We are able to extrapolate the relationship between the resonance frequency of the cantilever and the shunt capacitance as load.

$$f_n = \frac{1}{2\pi}\sqrt{\frac{3\left\{\left[\left(s_{11}^E - \frac{d_{31}^2 w_p L_p}{t_p C_p}\right)^{-1} + \left(s_{11}^E - \frac{d_{31}^2 w_p L_p}{t_p(C_p + C_s)}\right)^{-1}\right]\left[\frac{w_p t_p^3}{12} + w_p t_p\left(\frac{t_p + t_s}{2}\right)^2\right] + Y_s\frac{w_s t_s^3}{12}\right\}}{L^3\left(T_M + 0.24 m_b\right)}} \quad (1.44)$$

The natural frequency depends on the material properties (s_{11}^E, d_{31}), electromechanical coupling factor (k_{31}) and the structure geometry both substrate and piezoelectric elements. One piezo is used for energy harvesting while the second one for tuning the resonance frequency by changing parallel capacitance.

An important parameter is the tuning ratio, and it shows the maximum changed of the natural frequency with an adjustable load.

$$Tuning\ Ratio\ (\%) = \frac{f_{max} - f_{min}}{f_{min}} \times 100 \quad (1.45)$$

where:

- $\mathbf{f_{max}}$: maximum natural frequency
- $\mathbf{f_{min}}$: minimum natural frequency

1.5 PZN-5.5%PT vs PZT piezoelectric materials

This section describes the electrical parameters of the single crystal $PZN - 5.5\%PT$ (Lead Zinc Niobate-5.5% Lead Titanate) of Microfine Technologies Ltd [15] compared with PZT (Lead Zirconate Titanate) piezoelectric materials used by PI Ceramic [16].

Recently, it has been found that the ferroelectric single crystal materials near the Morphotropic Phase Boundary (MPB) composition, show larger electromechanical coupling factor (k_{31}) and charge coefficient (d_{31}) rather than the PZT elements [17]. Thus, an analytical evaluation has been done in order to verify this behaviour.

The most important aspect that is necessary to see, before to make the cantilever beam, is the *resonance frequency tuning ratio*. In fact, this value gives us an information on how much is possible to shift the piezoelectric resonance frequency.

Fig. 1.12 shows a pairs of PZN piezoelectric elements which have to be contacted (bonding wires) and supported by using an high stiffness substrate (Steel or Brass) before to use them as a cantilever beam. Fig. 1.13 presents a typical unimorph cantilever beam produced by PI Ceramic which is already built and contacted with electrodes.

Material	$\epsilon_{33}^{T}/\epsilon_{0}$	s_{11}^{E}[pm²/N]	s_{11}^{D}[pm²/N]	d_{31}[pC/N]	k_{31}
PZT-5.5%PT	4000	54	23.6	1100	0.75
PZT	1750	16.1	14.1	−180	0.35

Table 1.2: Parameters: PZN-5.5%PT Crystal type $[100]^{L}[0-11]^{W}[011]^{T}$ and PZT piezoelectric materials.

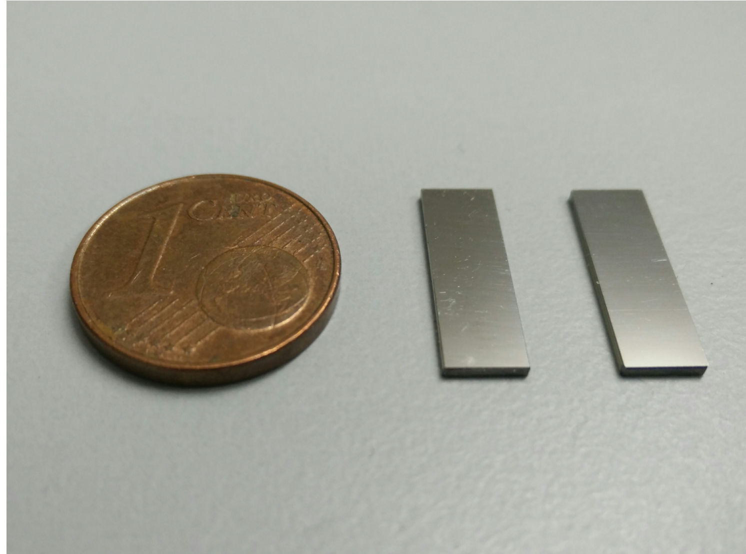

Figure 1.12: PZN-5.5%PT piezoelecric material.

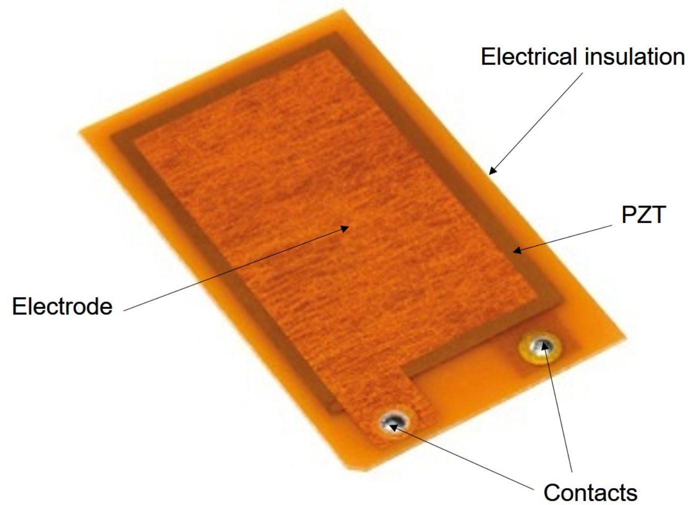

Figure 1.13: PI Ceramic cantilever beam with PZT piezoelectric material.

1.6 Tuning ratio: Analytical study

The structure size of the bimorph cantilever plays an important role on the tuning ratio. In order to build the beam, it is necessary to define the right dimensions of the structure for reaching an high tuning ratio.

By applying, on a MATLAB script, the equations shown in the previous section, it is possible to understand the behaviour of piezoelectric material. First of all, It was fixed the same length and width for both PZN piezoelectric materials and the steel, chosen as substrate. After that, two kind of evaluations have been done for knowing which piezoelectric material is suitable for my work.

In particular, for the first test, an hypothetical bimorph cantilever beam made with PZN material has been compared with three kinds of PI Ceramic known as: $A11$, $A12$, $A15$, where the difference between them are only the dimensions of the beam, Tab. 1.3. The analytical results, Fig. 1.14a, show a tuning ratio around 20% for the single crystal material and less than 5% for PZT elements. However, similar results are obtained by using a cantilever beam based on the same dimensions of the piezoelectric materials in exam, Tab. 1.4 and Fig. 1.14b.

As shown in Eq. 1.8, a higher electromechanical coupling factor (k_{31}) allows to increase the distance between the mechanical compliance in open circuit (s_{11}^D) and the mechanical compliance in short circuit (s_{11}^E). Hence, this effect extends the frequency shift and the tuning ratio in PZN-PT piezoelectric materials, which are chosen for my thesis.

Subsequently, the resonance frequency of the beam built with single crystal material, has been evaluated as function of the capacitance ratio. The results (Fig. 1.15), show an high resonance frequency, around 3500 Hz without using any tip mass on the cantilever. It is not useful for those applications where the bandwidth of the vibration goes down to few hundreds Hz. For this reason, I added a tip mas $T_M = 15\ g$ in order to reach a lower resonance frequency, around 400 Hz. Probably, is possible to add more tip mass for decreasing again the resonance frequency, but the risk of breaking the piezoelectric elements is much higher.

Beam	**L x W x T [mm]**	**Cp [nF]**
PZN-5.5%PT (Test cantilever)	15 x 5 x 0.8	3.4
PZT (A11 PI Ceramic)	50 x 30 x 0.1	150
PZT (A12 PI Ceramic)	50 x 30 x 0.2	90
PZT (A15 PI Ceramic)	50 x 30 x 0.5	45

Table 1.3: Dimensions and capacitance of piezoelectric materials: PZT used in PI Ceramic cantilever and PZN provided as sample from Microfine Technology Ltd.

Beam	L x W x T [mm]	Cp [nF]
PZN-5.5%PT (Test cantilever)	15 x 5 x 0.8	3.4
PZT (Test cantilever)	15 x 5 x 0.8	4.4

Table 1.4: PZT and PZN-5.5%PT piezoelectric elements with the same dimensions in order to evaluate their performance.

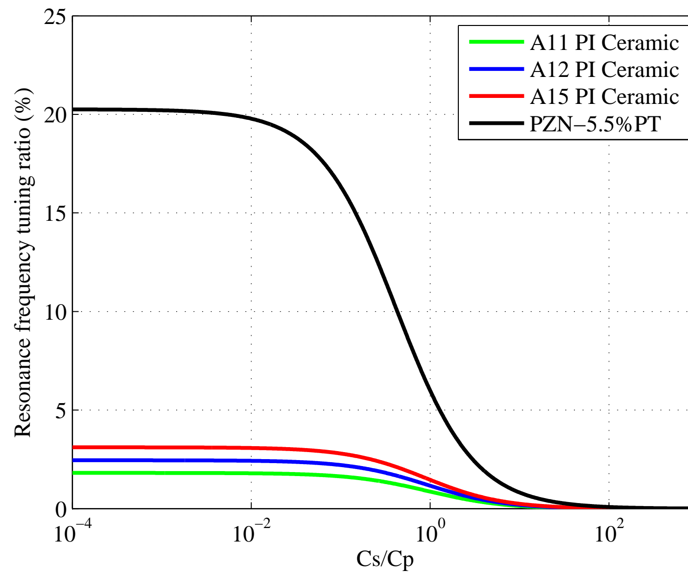

(a) Test cantilever made with PZN-5.5%PT compared with PI Ceramic beams.

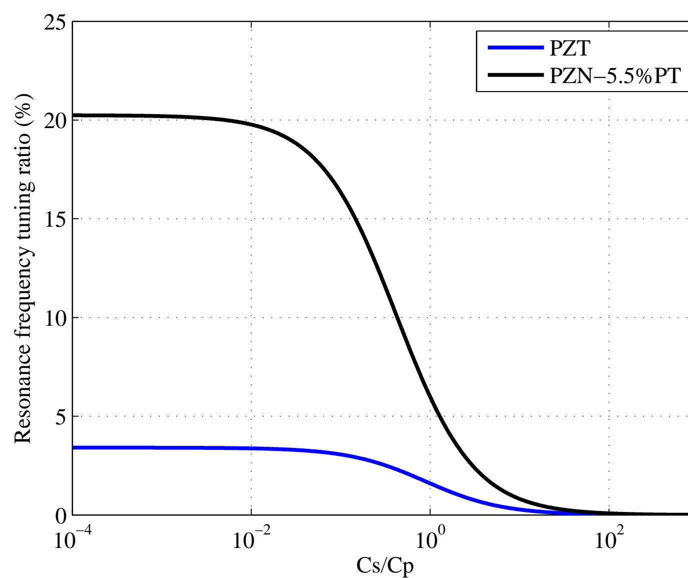

(b) Test cantilever made with PZT and PZN-5.5%PT of the same dimensions.

Figure 1.14

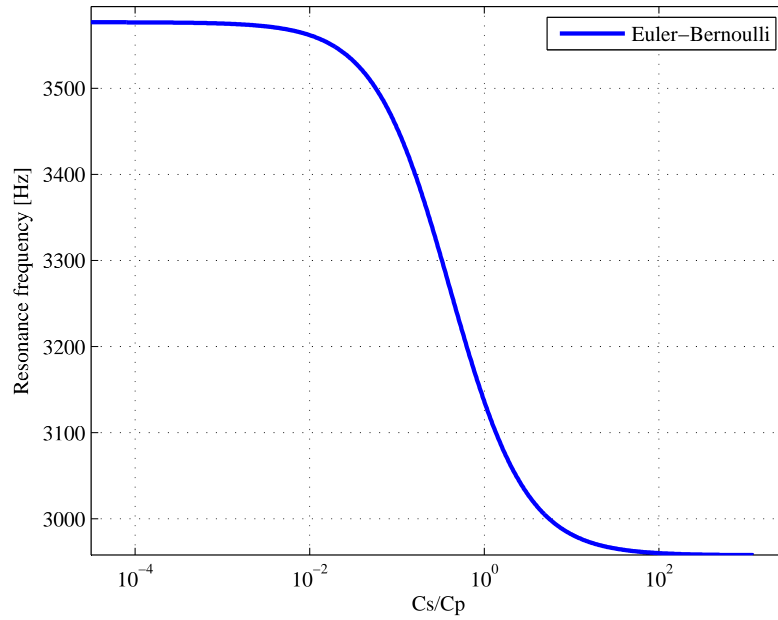

(a) without tip mass

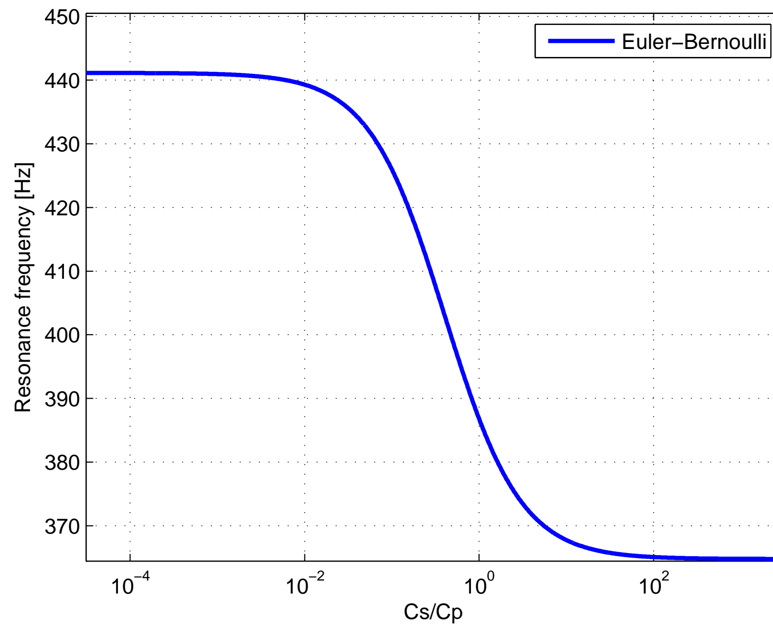

(b) with tip mass $T_M = 15\ g$

Figure 1.15: Resonance frequency as function of the capacitance ratio for PZN-5.5%PT piezoelectric materials.

Chapter 2

Bimorph cantilever manufacturing

2.1 Fabrication process

By using the single crystal PZN-5.5%PT provided from Microfine Technology of Singapore, a bimorph cantilever hase been developed [18] for energy harvesting purpose, Fig. 2.1.

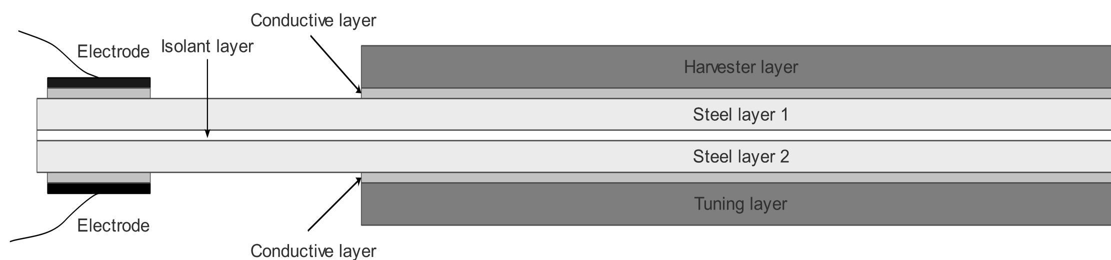

Figure 2.1: Bimorph Cantilever

Due to the brittleness of the piezoelectric elements, the electrodes has been applied before bonding all layers. The dimension of the *steel layer* [19] is chosen by evaluating the resonance frequency.

The tuning ratio and the effective stiffness of the structure depend also on the thickness ratio (ts/tp) between the substrate and the piezoelectric layers. This effect is shown in Fig. 2.2, where it is easy to see that, in order to optimize the tuning ratio, the thickness of the active part has to be the same order or higher than the thickness of the shim layer (substrate).

However, maximizing the thickness of the piezo is not a viable solution because it is already fixed by the manufacturer. For this reason, I minimized the thickness

of the shim layer by avoiding to decrease the quality factor of the whole structure.

In fact, all those materials used as substrate, have an high quality factor and in general a higher mechanical stiffness than the piezoelectric ones.

Anyway, it represents a limit for the thickness reduction and for working in a good point of the characteristic, it has been chosen the following thickness ratio:

$$\frac{t_s}{t_p} = 0.5 \tag{2.1}$$

.

Subsequently, I soldered small wires on a thin copper film ($tc = 100\mu m$) in order to build the electrodes. After that, I fixed the copper on the steel with a *conductive glue* (Chemtronics CW2400 [20]). It is composed from two different part, the first one (A) is made with a silver powder while the second one (B) is a glue. Both have to be mixed in equal amount ($1:1$) by weight and volume for 2 minutes and applied within 8 minutes.

Before to apply the glue, it is important to clean very well the surface in order to remove any contamination which may prevent adequate material contact. After to have bounded them, the curing time and electrical conductivity depend primarily on temperature. At the beginning the Epoxy was cured at room temperature for 4 hours. This was not a good solution because between the steel and copper there were about 10 Ω of resistivity or more. The reason is written in the datasheet, for faster curing times, maximum conductivity and adhesion, it is necessary to cure the bond between $65 - 121°C$ for $5 - 10$ minutes. For this reason, I cured it at $80°C$ with an heating plate in order to solve the problem.

After that, the steel layers were bounded together with a generic non-conductive glue for making it really insulating. Finally, the piezoelectric materials and the steel layers are joined with the conductive glue in the same approach over illustrated.

	Material	**LxWxT [mm]**
Piezoelectric element	PZN-5.5%PT	$15.0 \times 5.0 \times 0.8$
Shim layer	Steel	$30.0 \times 5.0 \times 0.2$
Electrode	Copper	$5.0 \times 5.0 \times 0.07$
Conductive Layer	CW2400	$25.0 \times 5.0 \times 0.04$
Non-Conductive layer	Super glue	$40.0 \times 5.0 \times 0.08$

Table 2.1: Cantilever beam dimensions with PZN-5.5%PT Crystal type: $[100]^L[0-11]^W[011]^T$.

Material	Young's Modulus [10^9N/m^2]	density [Kg/m^3]
PZN-5.5%PT	50.4	8500
Steel	1.6	7500

Table 2.2: Young's modulus and density both steel layers and piezoelectric materials.

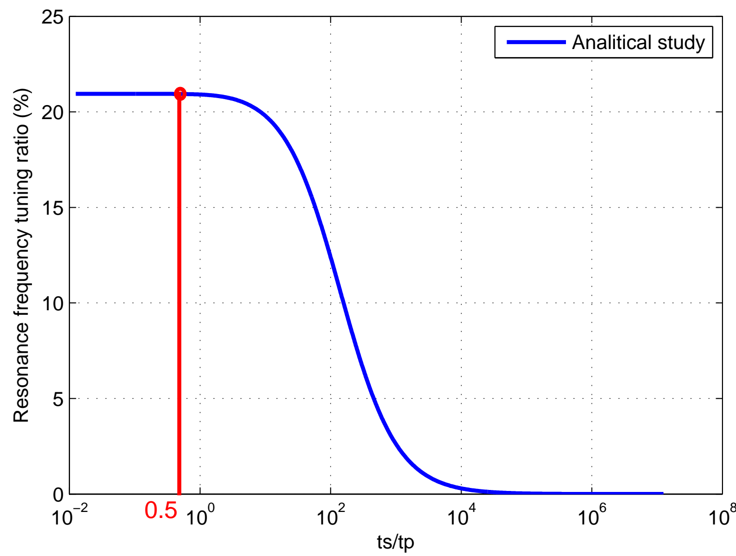

Figure 2.2: Resonance frequency tuning ratio as function of the thickness ratio.

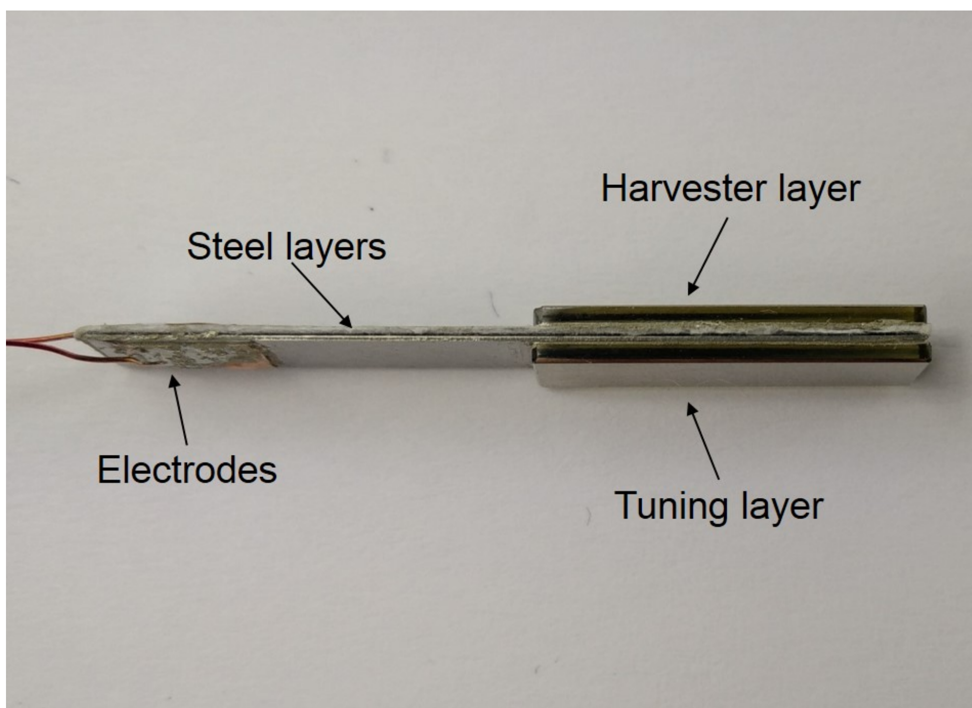

Figure 2.3: Real bimorph cantilever.

2.2 Harvester

The last two electrodes of the piezoelectric elements were placed on the structure used for clamping the cantilever beam, Fig. 2.4, in order to preserve the crystals as much as possible.

The structure is made with an aluminium base which has four holes for fixing it to the electrodynamic shaker. The second part is composed by plastic material where a little slot is placed, on the top of Fig. 2.6, for preserving the integrity of both piezoelectric elements once they are clamped.

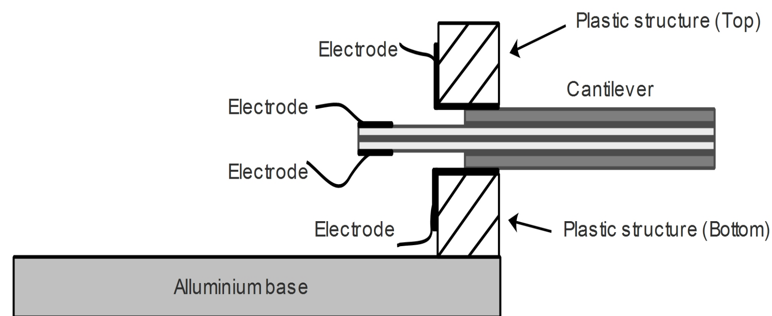

Figure 2.4: A section of the structure used for clamping the cantilever beam.

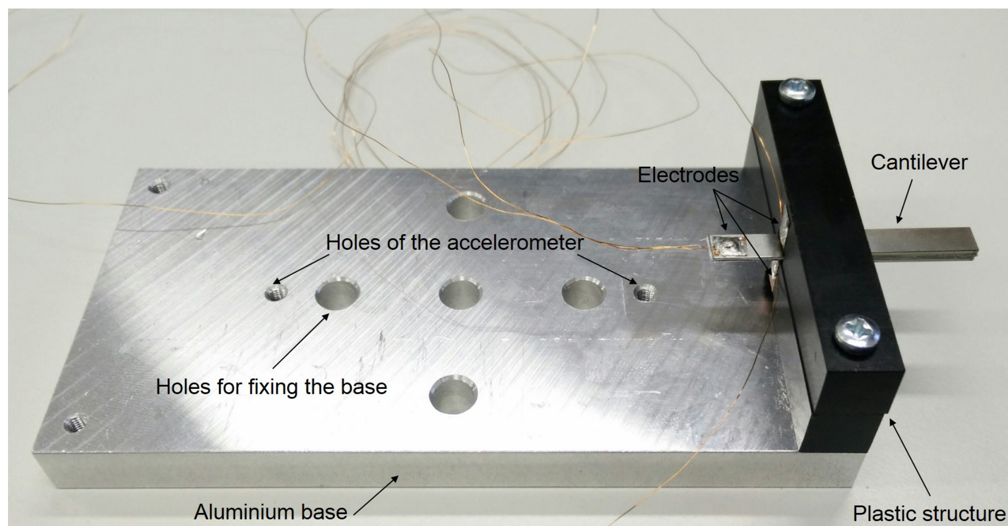

Figure 2.5: Top view of the Harvester.

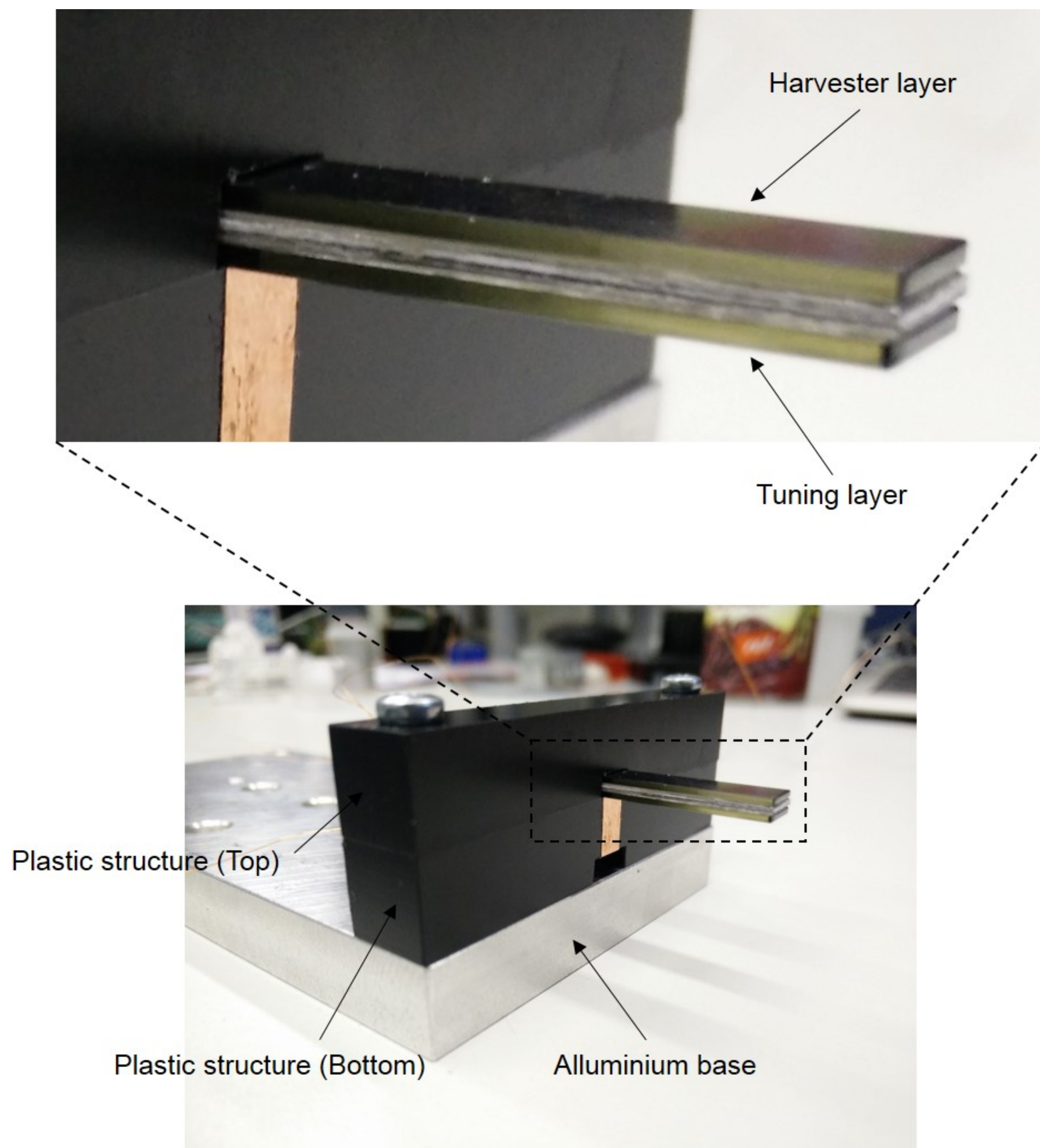

Figure 2.6: Front view of the Harvester.

Chapter 3

Measurements with Electrodynamic shaker

3.1 Test stand for measurements

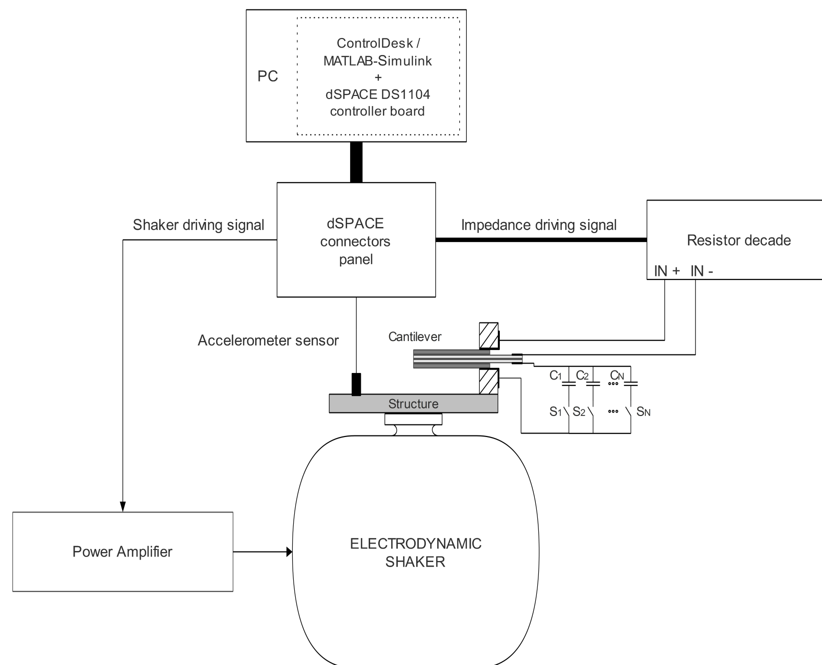

Figure 3.1: Test stand for measurement with electrodynamic shaker.

The test stand for measurement with the vibration exciter, allows to evaluate the output power of the harvester as function of a variable impedance load and the

vibration frequency, by applying different values of shunt capacitance. Hence, the resonance frequency tuning ratio is measured experimentally.

It is composed by:

- dSpace board
- Power amplifier
- Impedance load
- Electrodynamic shaker
- Harvester with shunt capacitance
- Accelerometer sensor
- Control desk software / MATLAB-Simulink

Basically, the heart of the system is the *dSPACE DS1104 board* [21], Fig. 3.2a, which is used for rapid control prototyping. This $PCIe$ controller board upgrades the functionalities of the laboratory computer, by introducing a PowerPC technology ($PPC603e$) with a 64-bit floating point processor $MPC8240$ and CPU clock at 250 MHz, for real-time application.

The *controller board* is connected to the *connector panel*, Fig. 3.2b, by using a ribbon cable [22]. It provides the access to I/O channels for analog signals via BNC connectors (ADC/DAC ports) and digital signals via Sub-D connectors.

Subsequently, the signals pass through the *power amplifier* for driving the *electrodynamic shaker* S 52110 manufactured by TIRA GmbH, Fig. 3.2d. The power amplifier used in this thesis is the model $BAA120$ (Fig. 3.2c), manufactured from the same company of the vibration exciter. The amplifier has to provide the right energy to the electrodynamic shaker, as function of the control loop system running on the dSPACE board, in order to keep the required vibration on the top of the shaker. The Real-Time interface (RTI) is fully programmable in MATLAB-Simulink®by using a block diagram environment, where all I/O signals are configured graphically with dSPACE libraries. Hence, a control loop algorithm was compiled in C code and downloaded directly on the dSPACE hardware. The debugging can be done on the *ControlDesk* software, which is useful for seeing in real-time the variables under investigation [23].

Furthermore, a *resistor decade* provides the possibility to change the resistance load on the cantilever beam, driven by the controller board. Finally, the harvester is placed on the electrodynamic shaker and connected to an accelerometer sensor as feedback for the control system.

(a) dSPACE controller board.

(b) dSPACE connector panel.

(c) Power amplifier TIRA BAA120.

(d) VIbration excider TIRA vib S 52110.

Figure 3.2: Main bench equipments of the whole system.

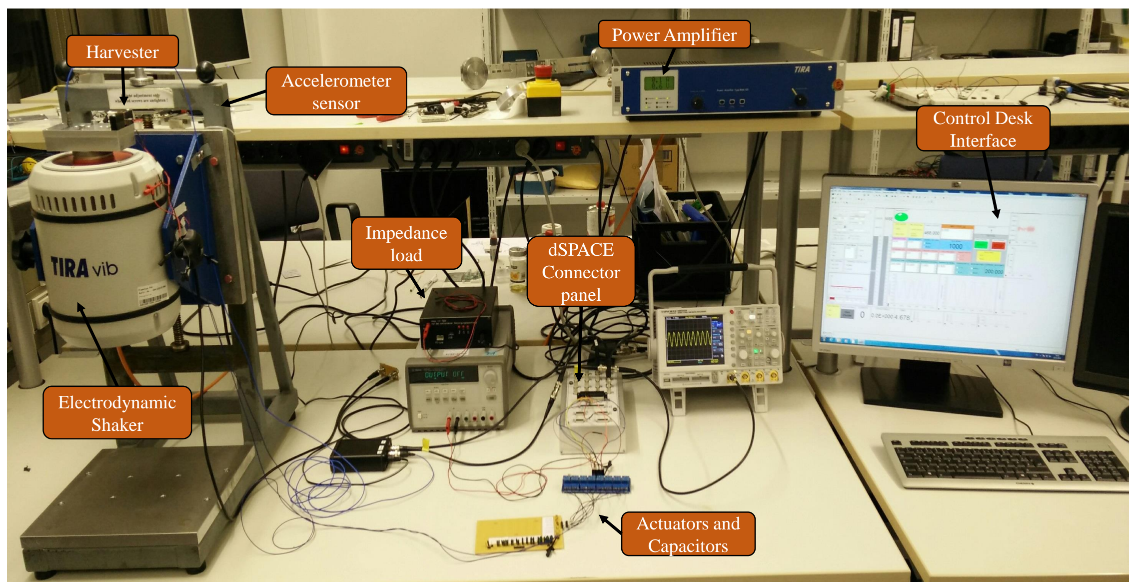

Figure 3.3: Real set up for measurement with electrodynamic shaker.

3.2 Piezoelectric output power

Basically, before taking the measurement, it is necessary to evaluate the *dynamic response* of the beam. Then, we are able to understand which frequency the piezoelectric materials are going to resonate and, at the same time, if the cantilever is clamped on the structure in the right way.

Fig. 3.4 shows the damping of one layer of piezoelectric element, with a typical response of under-damped system [24].

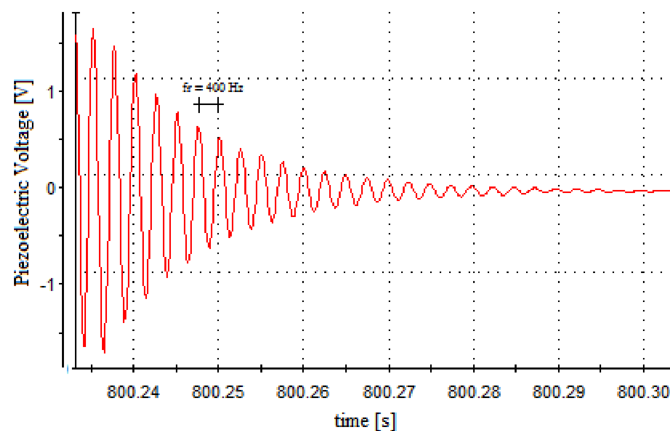

Figure 3.4: Piezoelectric damping.

The output power is the first measurement conducted on piezoelectric materials for knowing their behaviour as function of the frequency and the impedance load.

Fig. 3.5 shows the ControlDesk interface used where it is possible to set two different *use modes*: a *frequency sweep* between two frequencies of interest or a *single frequency*. In both cases, a sinusoidal waveform is reproduced on the top of the shaker which amplitude (g) is defined on the same interface.

The piezoelectric voltage is brought to the resistor decade which provides the possibility to make a resistance sweep or to fix one desired load. Then, the output power is evaluated by running a frequency sweep for each resistance load or vice versa:

	without C_s	**with $C_s = 22$uF**
Amplitude acceleration [g]	0.5	0.5
Tip mass [g]	15	15
Impedance sweep [kΩ] (tuning layer)	5-1600	5-1600
Frequency sweep [Hz] (harvesting layer)	400-500	360-460

Table 3.1: Set up for measurement.

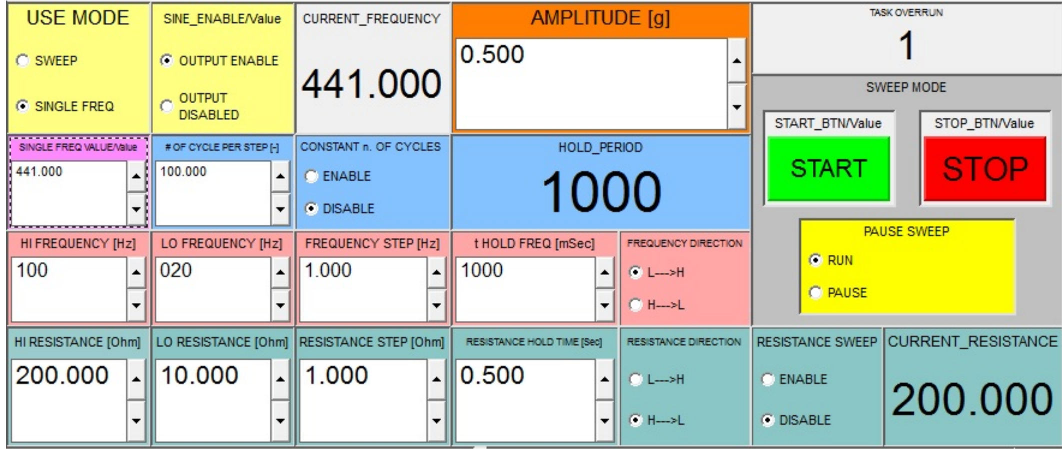

Figure 3.5: ControlDesk inferface for measurement with electrodynamic shaker.

Hence, the maximum power has been found for a particular load and frequency, Fig. 3.6. These results are collected in Tab. 3.2 and the tuning ratio is calculated by taking the resonance frequency in both condition, with and without shunt capacitance:

$$Tuning\ Ratio = \frac{fr_{max} - fr_{min}}{fr_{min}} = \frac{446 - 404}{404} = 10.4\% \tag{3.1}$$

Subsequently, I replaced the resistor decade and fixed the load for the maximum power between the harvesting layer and the connector panel, Fig. 3.7.

Due to, the input impedance of the connector board ($R_{in} = 1\ M\Omega$), I added in parallel a resistance R which value is:

$$R_{//} = R_{in}//R = 270\ k\Omega \quad \Rightarrow \quad R = 369.8k\Omega \tag{3.2}$$

Then, the piezoelectric layer is able to see 270 $k\Omega$ in order to reach the maximum power. Now, the output voltage of the piezo is recorded directly with the ControlDesk and managed by MATLAB/Simulink.

	without C_s	**with C_s = 22uF**
Impedance load [kΩ]	276.51	276.51
Output Power [μW]	161.9	155.6
Resonance frequency [Hz]	446	404

Table 3.2: Results at maximum output power of the harvesting layer.

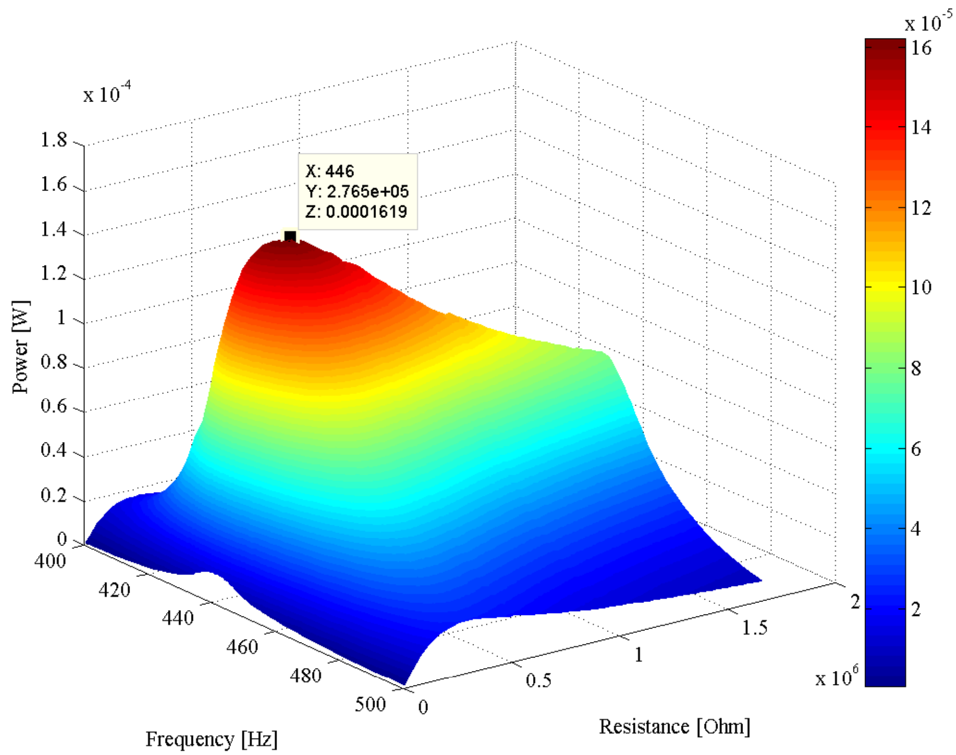

(a) without shunt capacitance

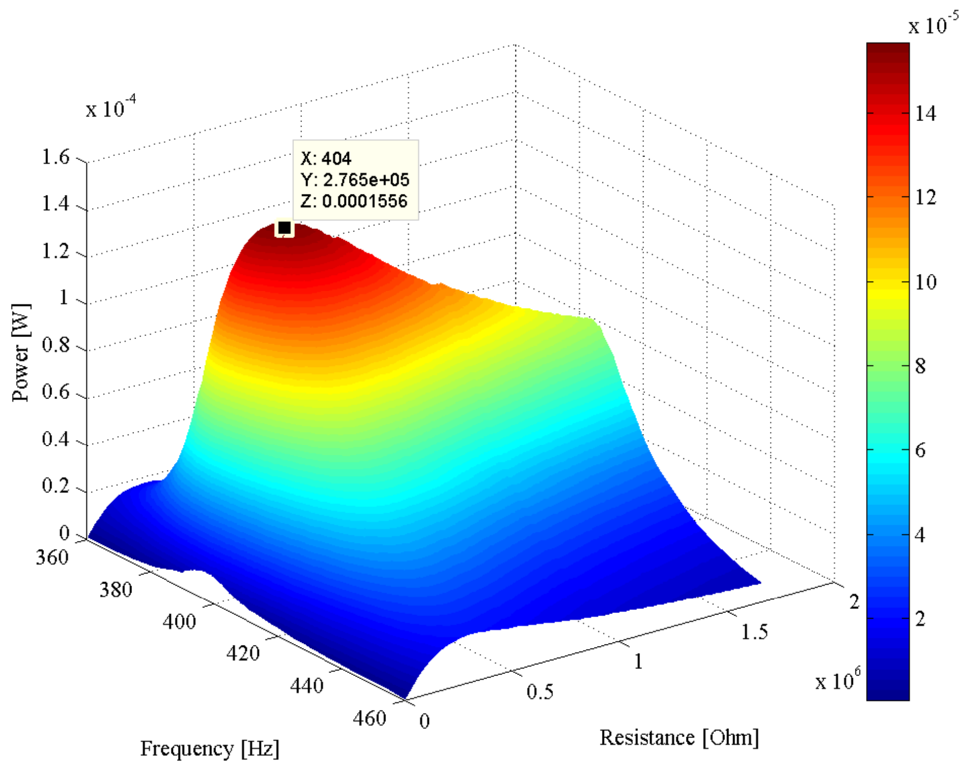

(b) with $C_s = 22uF$

Figure 3.6: Output power of harvesting layer with and without shunt capacitance.

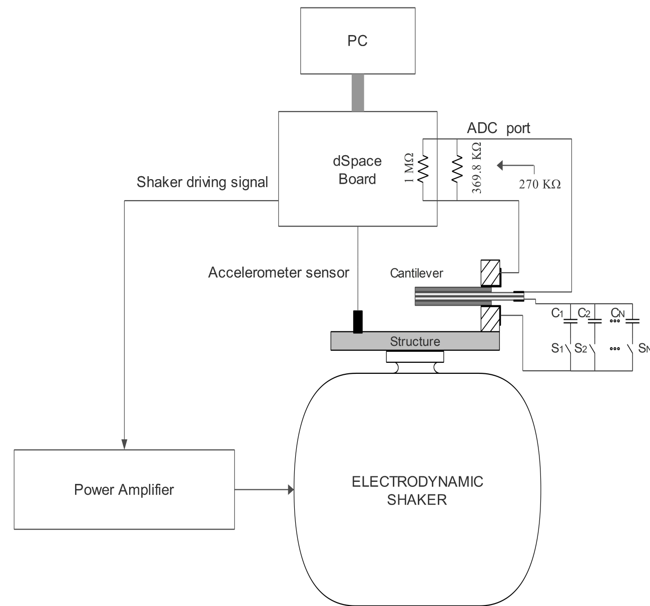

Figure 3.7: Test stand for measurement with electrodynamic shaker and fixed load.

3.3 Tuning ratio: experimental results

With the test stand modified in the previous section, the last measurement have been done for evaluating the piezoelectric tuning ratio in three different situation:

- *Series connection* of both piezoelectric layers
- *Parallel connection* of both piezoelectric layers
- *Electrical tuning* of a piezoelectric layer

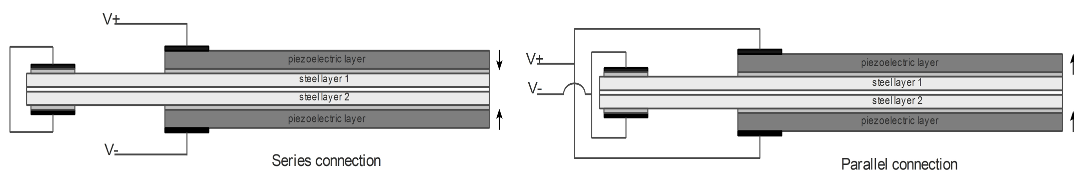

Figure 3.8: Series and parallel connections of piezoelectric elements.

The output power of Fig. 3.9, shows different bandwidth for each configuration, collected in Tab. 3.4. In particular, by moving the resonance frequency with a shunt capacitance, we obtained a $\Delta f = 75\,Hz$ and $Tuning\ Ratio = 10.5\,\%$ as beforehand. Instead, the series and parallel connections offer an higher output

power compared with that one reached from only one piezoelectric element, while the bandwidth got with the combination of both (series and parallel) is pretty similar to the bandwidth got with an electrical tuning, by using shunt capacitance.

Then, two ways can be followed in order to have a wideband generator for keeping the maximum power: *switching among series and parallel connection* or *making an electrical tuning of the cantilever beam resonance frequency.*

Although, thinking an algorithm for the first solution could be faster rather than the second one, but, that approach doesn't permit to match the resonance frequency with the vibration frequency. Anyway, this thesis is focused on making an algorithm for the second approach where an electrical tuning is used.

Furthermore, the tuning ratio achieved is a bit lower than analytic one, Fig. 3.11. The reason is inside the beam fabrication process. The stiffness of the whole structure play an important role on the tuning ratio, in fact, the glues (conductive and non-conductive) used for bonding the steel layers and the piezoelectric materials, have a lower stiffness compared with the substrate and crystals ones.

Thus, by changing the manufacturing with other solutions, the bandwidth could increase. For example, the double substrate of steel can be replaced with only one steel layer (or Brass with a higher stiffness), in order to improve the quality of the all structure, by removing on layer of glue. By the way, the analytical study with Euler-Bernoulli has an intrinsic limitation because of the model besides the piezoelectric parameters uncertainty. In fact, a 10 % of parameters variation has already a big effect on the tuning ratio. For all these reasons, there is such difference between the measurement and the mathematical study.

In a small range of shunt capacitance, the resonance frequency has a linear behaviour and the effect of the electrical load on the structure is stronger against the noise. Then, it is useful to work there with the MPPT algorithm for moving the resonance frequency, Section 5.

Amplitude acceleration [g]	0.5
Frequency sweep [Hz]	350-500
Tip mass [g]	15
Load (harvester layer) [kΩ]	270
Load (tuning layer)	shunt capacitance (C_s)

Table 3.3: Technical data for measurement.

	Series c.	**Parallel c.**	**Series c.+Parallel c.**	**Electrical tuning**
Δf [Hz]	51.5	57	74	75

Table 3.4: Bandwidth at 50 % of the maximum power/voltage.

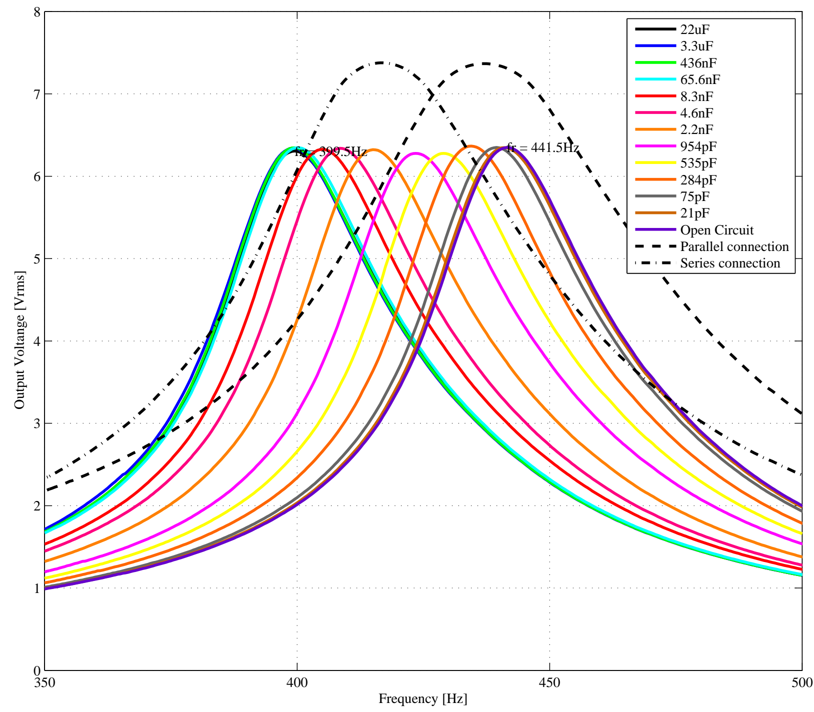

(a) Output voltage

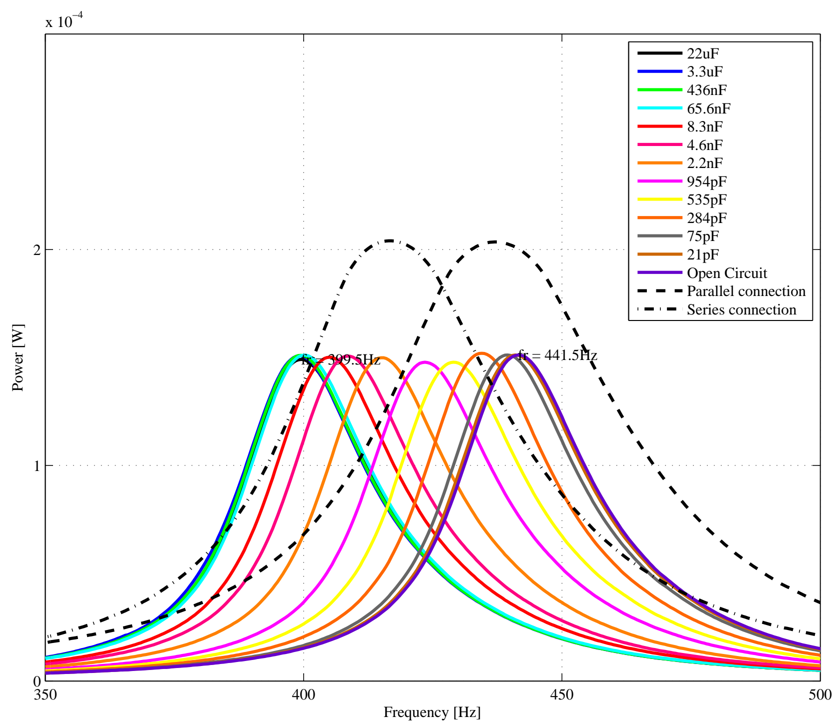

(b) Output Power

Figure 3.9: Output piezoelectric harvesting layer with and without Cs.

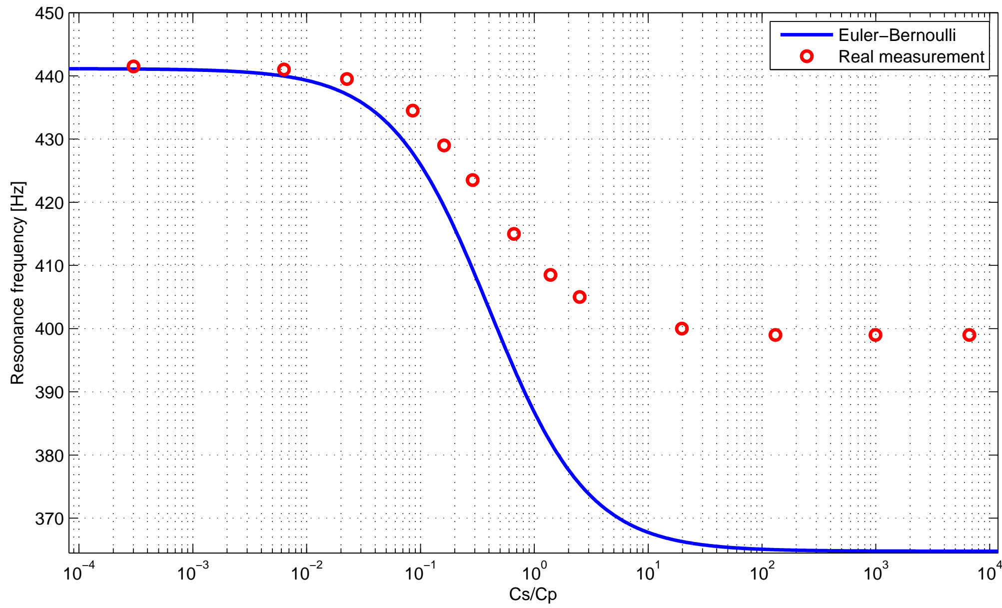

Figure 3.10: Resonance frequency tuning ratio as function of the capacitance ratio C_s/C_p by comparing both analytical model and real measurement.

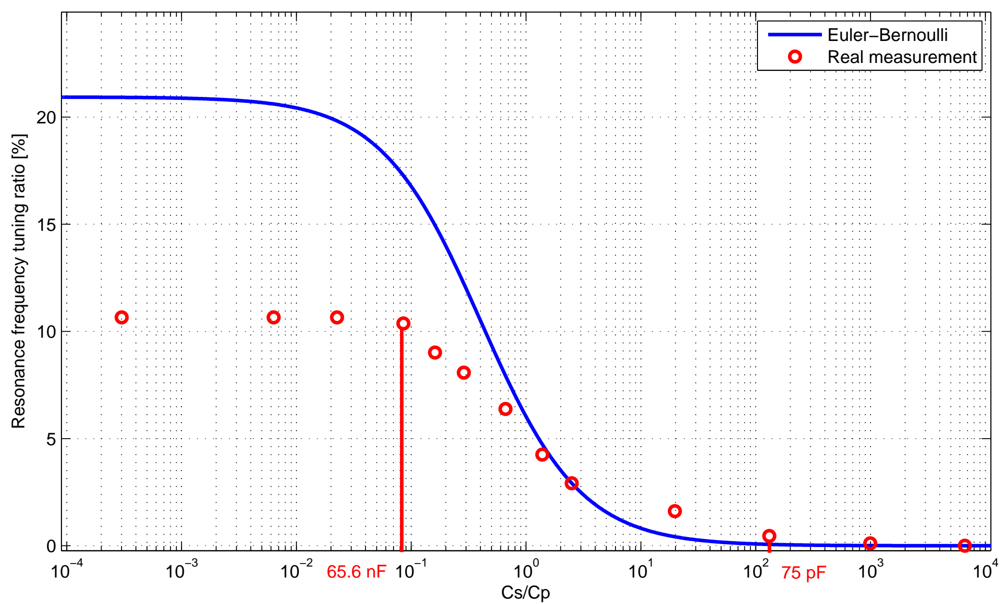

Figure 3.11: Tuning ratio % as function of the capacitance ratio C_s/C_p by comparing both analytical model and real measurement.

Chapter 4

Electrical equivalent circuit

4.1 General background

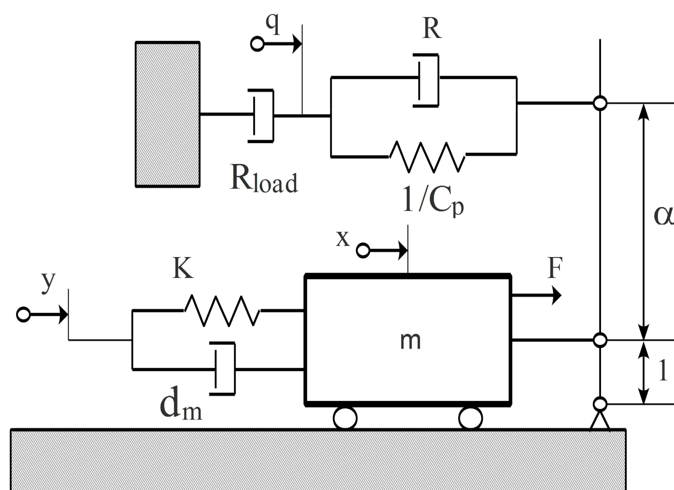

Figure 4.1: Piezoelectric mechanical model.

Parameters:

- **m**: equivalent mass
- $\mathbf{d_m}$: equivalent mechanical damping
- **K**: equivalent mechanical stiffness
- **F**: applied force

- **x**: displacement of the mass
- **y**: displacement at the base-motion of the harvester
- **q**: electric charge
- $\mathbf{C_p}$: piezoelectric capacitance
- **R**: electric losses inside the piezoelectric material
- $\mathbf{R_{load}}$: resistive load
- $\boldsymbol{\alpha}$: transmission factor

The electro-mechanical model for piezoelectric elements [25], Fig. 4.1, allows to evaluate the output power of the system and provides all information in order to understand the behaviour of the cantilever beam, as function of the frequency. This model is valid by considering a piezoelectric generator mechanically stimulated, which produces an electric energy. In particular, the mechanical displacement is related with the electrical charge.

The mechanical model is based on a single degree of freedom besides it is also represented as electrical model of Fig. 4.2. The equivalent mass (m) can be described as an inductance (L_m), the mechanical stiffness (K) represents a capacitance (C_m) and finally the damping (d_m) is the equivalent of a resistor (R_m). The mechanical part is coupled with the electrical one by α, which is called transmission factor.

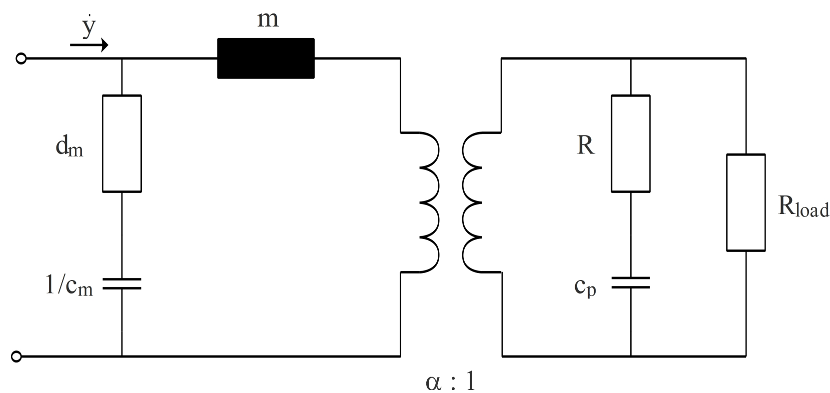

Figure 4.2: Piezoelectric electrical model.

$$L_m = \frac{m}{\alpha^2} \tag{4.1}$$

$$C_m = \frac{\alpha^2}{K} \tag{4.2}$$

$$R_m = \frac{d_m}{\alpha^2} \tag{4.3}$$

By the way, the behaviour of a piezoelectric ceramic can be studied with the *Van Dyke model* [26], Fig. 4.3, which is valid only near at the resonance frequency as well as the model in Fig. 4.2.

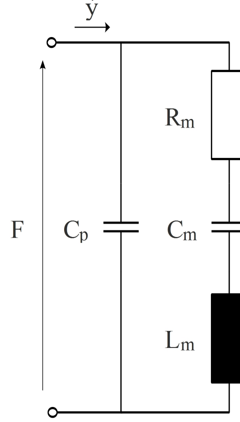

Figure 4.3: Butterworth-van Dyke model.

The admittance of the electrical circuit is expressed as follow:

$$Y(j\omega) = G + jB \tag{4.4}$$

where:

- **G**: conductance
- **B**: susceptance

$$G = Re\{Y(j\omega)\} = \frac{C_m^2 R_m \omega^2}{C_m^2 R_m^2 \omega^2 + (C_m L_m \omega^2 - 1)^2} \tag{4.5}$$

$$B = Im\{Y(j\omega)\} = \frac{\omega C_m (1 - C_m L_m \omega^2)}{1 + C_m \omega^2 (C_m R_m^2 + L_m (C_m L_m \omega^2 - 2))} + \omega C_p \tag{4.6}$$

The resistance R (electric losses) is negligible.

Hence, the first step for characterizing the ceramics is to find out the value of all parameters $[L_m, C_m, R_m, C_p]$ presented in the model. Fig. 4.4 shows the admittance Bode and Nyquist diagrams of a typical piezoelectric response [27], where all frequencies of interest are marked and used for calculating the parameters:

- $\mathbf{f_s}$ = series frequency
- $\mathbf{f_p}$ = parallel frequency
- $\mathbf{f_n}$ = frequency of minimum admittance or maximum impedance
- $\mathbf{f_m}$ = frequency of maximum admittance or minimum impedance
- $\mathbf{f_r}$ = resonance frequency
- $\mathbf{f_a}$ = antiresonance frequency

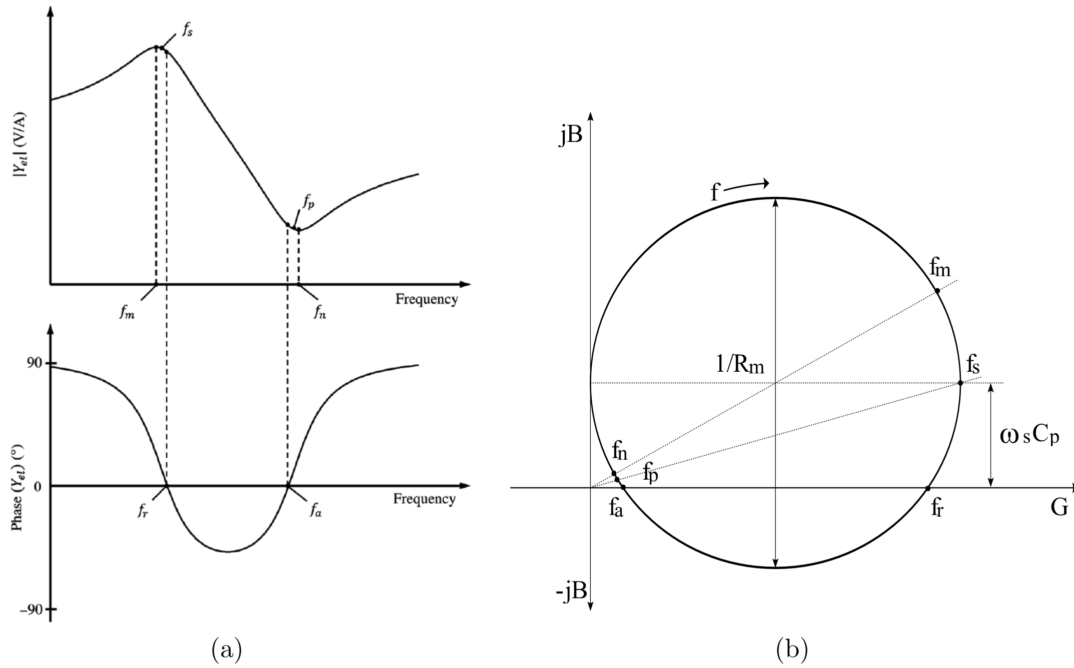

Figure 4.4: (a) Admittance (Bode modulus and phase) diagrams of a piezoelectric material; (b) Admittance Nyquist diagram of a piezoelectric material.

An *impedance analyzer* is needed in order to get both Bode and Nyquist plot. From the real measurement, led on the cantilever beam studied in this thesis, C_p and R_m are extrapolated by using the real part (G) and imaginary part (B) of the admittance, Fig. 4.4b.

$$C_p = \frac{max(B) - min(|B|)}{2\omega_s} \tag{4.7}$$

$$R_m = \frac{1}{max(G) - min(G)} \tag{4.8}$$

The frequencies f_r, f_p, f_n are close to each other as well as f_a, f_s, f_m between them. Their difference depends on the internal losses (R_m). The value of the motional frequency (f_s) and the parallel frequency (f_p) are taken directly from the impedance measurement:

$$f_s = f[max(Re\{Y(j\omega)\})] \tag{4.9}$$

$$f_p = f[max(Re\{Z(j\omega)\})] \tag{4.10}$$

However, they can be computed as follow [27]:

$$\begin{cases} f_s = \dfrac{1}{\sqrt{L_m C_m}} \\ f_p = \dfrac{1}{L_m \dfrac{C_p C_m}{C_p + C_m}} \end{cases} \tag{4.11}$$

By resolving the previous system of equations, there are just two unknown variables, C_m and L_m:

$$C_m = C_p\left(\frac{f_p^2}{f_s^2} - 1\right) \tag{4.12}$$

$$L_m = \frac{1}{C_p(2\pi f_s)^2} \tag{4.13}$$

Although all parameters are known and the model is completed, an *optimizazion algorithm* is necessary for minimizing the difference between the model and the experimental data. It will be discussed in the following sections.

4.2 Test stand for measurements

Basically, the test stand, Fig. 4.5, is composed of the following parts:

- Harvester
- Shunt capacitance
- Faraday cage
- Impedance Analyzer
- Nova software for data processing

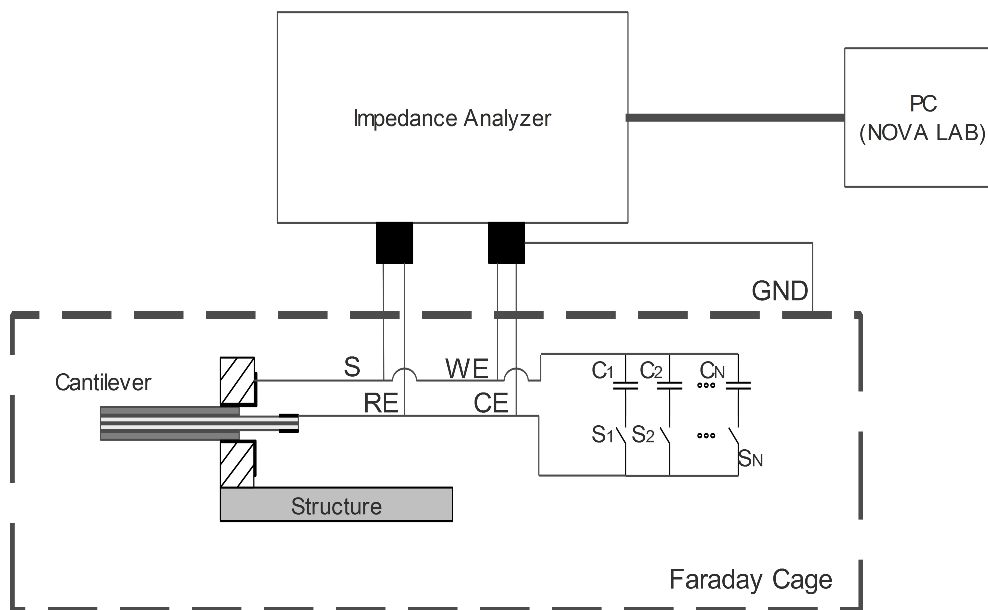

Figure 4.5: Test stand for impedance measurement.

The *harvester* is placed inside a *faraday cage* for external noise reduction which can influence the measurement. Then, a tip mass of $15g$ was added on the cantilever beam in order to lower its resonance frequency.

The impedance measurements were executed with *Autolab PGSTAT302N* of Metrohm [28], Fig. 4.6, which has a modular high power potentiostat/galvanostat [29] with features shown in Tab. 4.1. The instrument is used in a *two-electrode setup* and four probes:

- **CE**: Counter electrode

Figure 4.6: Autolab PGSTAT302N potentiostat/galvanostat.

Electrode connections	2, 3, and 4
Potential range	$\pm 10V$
Compliance voltage	$\pm 30V$
Maximum current	$\pm 2A$
Current ranges	$1A$ to $10nA$, in 9 dedades
Potential accurancy	$\pm 0.2\%$
Potential resolution	$0.3\mu V$
Current accurancy	$\pm 0.2\%$
Input impedance	> 1 TΩ
Potentiostat bandwidth	1 MHz

Table 4.1: Autolab PGSTAT302N features.

- **RE**: Reference electrode
- **WE**: Working electrode
- **S**: Sense
- **GND**: Ground connection

The system works by giving a sinusoidal voltage at one piezoelectric layer between two electrodes, RE and S, while the current flows through WE and CE.

Then, the impedance is evaluated with the simple *Ohm's law* and all results are stored in Nova software, which is developed by the same company of the instrument. A *procedure* is created for getting the measurement, Fig. 4.7, where is possible to set up some parameters among which the frequency sweep, numbers of steps, the type of wave and its amplitude.

The measurement is totally automatized and it provides the Bode and Nyquist diagrams useful for my evaluation.

Frequency range
First applied frequency 400 Hz
Last applied frequency 420 Hz
Number of frequencies 50
Significant digits 5

Amplitude
Amplitude 0.5
RMS

Integration time calculation
Integration time (maximum) 0.05 s
Integration cycles (minimum) 5

Frequency step
Linear
Logarithmic
Square root
Frequencies per decade

Wave type
Single sine
5 sines
15 sines

Replace Add Clear

	Frequency (Hz)	Amplitude ()	Wave type	Integration time	Minimum number of cycles to integrate
1	400	0.5	Single sine	0.05	5
2	400.04	0.5	Single sine	0.05	5
3	400.08	0.5	Single sine	0.05	5
4	400.12	0.5	Single sine	0.05	5
5	400.16	0.5	Single sine	0.05	5
6	400.2	0.5	Single sine	0.05	5
7	400.24	0.5	Single sine	0.05	5

OK Cancel

Figure 4.7: Autolab Nova software: Set up for measurement

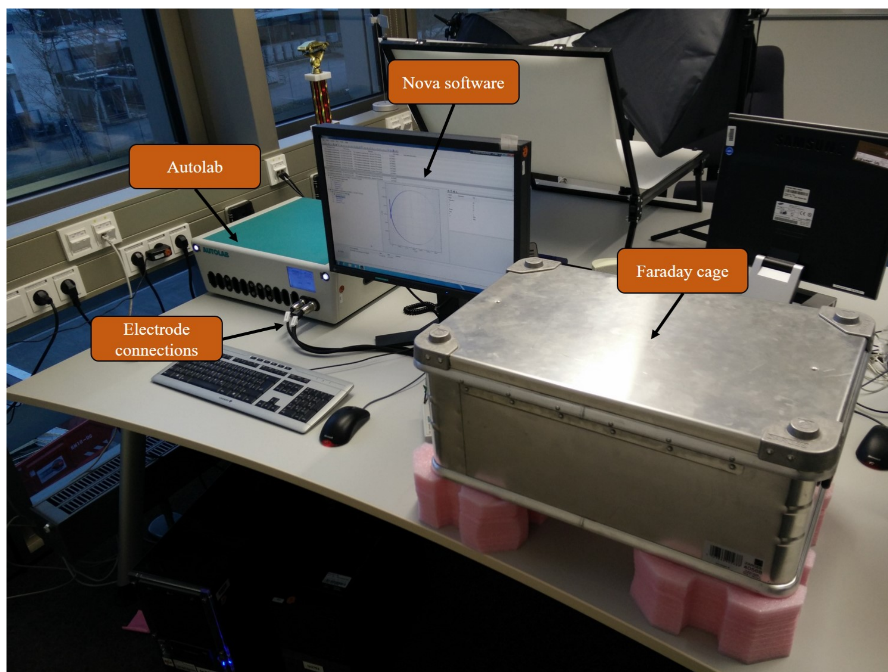

Figure 4.8: Real test stand for measurement.

4.3 Impedance measurements

The cantilever beam built in my thesis, is evaluated with impedance measurements for getting all parameters needed, in order to complete the electrical circuit. For this reason, Bode and Nyquist diagrams are shown in this section.

In particular, different shunt capacitance have been added in parallel to the tuning layer for understanding the behaviour of the harvester, as function of the frequency. Then, the parallel frequency (f_p) in (4.11), can be rewritten as follow:

$$f_p = \frac{1}{L_m \frac{(C_p + C_s)C_m}{C_p + C_s + C_m}} \tag{4.14}$$

As shown in Tab. 4.2, by increasing the value of the shunt capacitance (C_s), the parallel frequency lowers close to the series frequency which is mostly stable. That means, once chosen a shunt capacitance, the cantilever has a resonance frequency between f_n and f_m given by the configuration.

Hence, a tuning ratio of about 10% is still reached:

$$\begin{cases} f_{n1} = 443.87Hz & \text{without } C_s \\ f_{m7} = 405.10Hz & \text{with } C_s = 174nF \end{cases} \tag{4.15}$$

$$Tuning\ Ratio = \frac{f_{n1} - f_{m7}}{f_n 1} = 9.6\% \tag{4.16}$$

I stopped my measurements with $C_s = 174nF$, Fig. 4.13, because the admittance circle becomes smaller until it disappears when the shunt capacitance is too high.

In that case, the frequencies of interest are not defined.

Config.	**Shunt Capacitance**	$\mathbf{f_m}$**[Hz]**	$\mathbf{f_n}$**[Hz]**	$\mathbf{f_s}$**[Hz]**	$\mathbf{f_p}$**[Hz]**
1	without C_s	401.93	443.87	404.88	441.10
2	535pF	403.78	436.82	407.13	433.15
3	954pF	403.10	432.88	406.96	428.68
4	2.2nF	401.82	426.45	406.93	421.05
5	8.25nF	399.95	419.52	407.01	412.14
6	142nF	402.9	409.30	406.95	406.95
7	174nF	405.10	407.87	406.88	406.88

Table 4.2: Frequencies of interest evaluated by adding different shunt capacitance on the tuning layer of the cantilever beam.

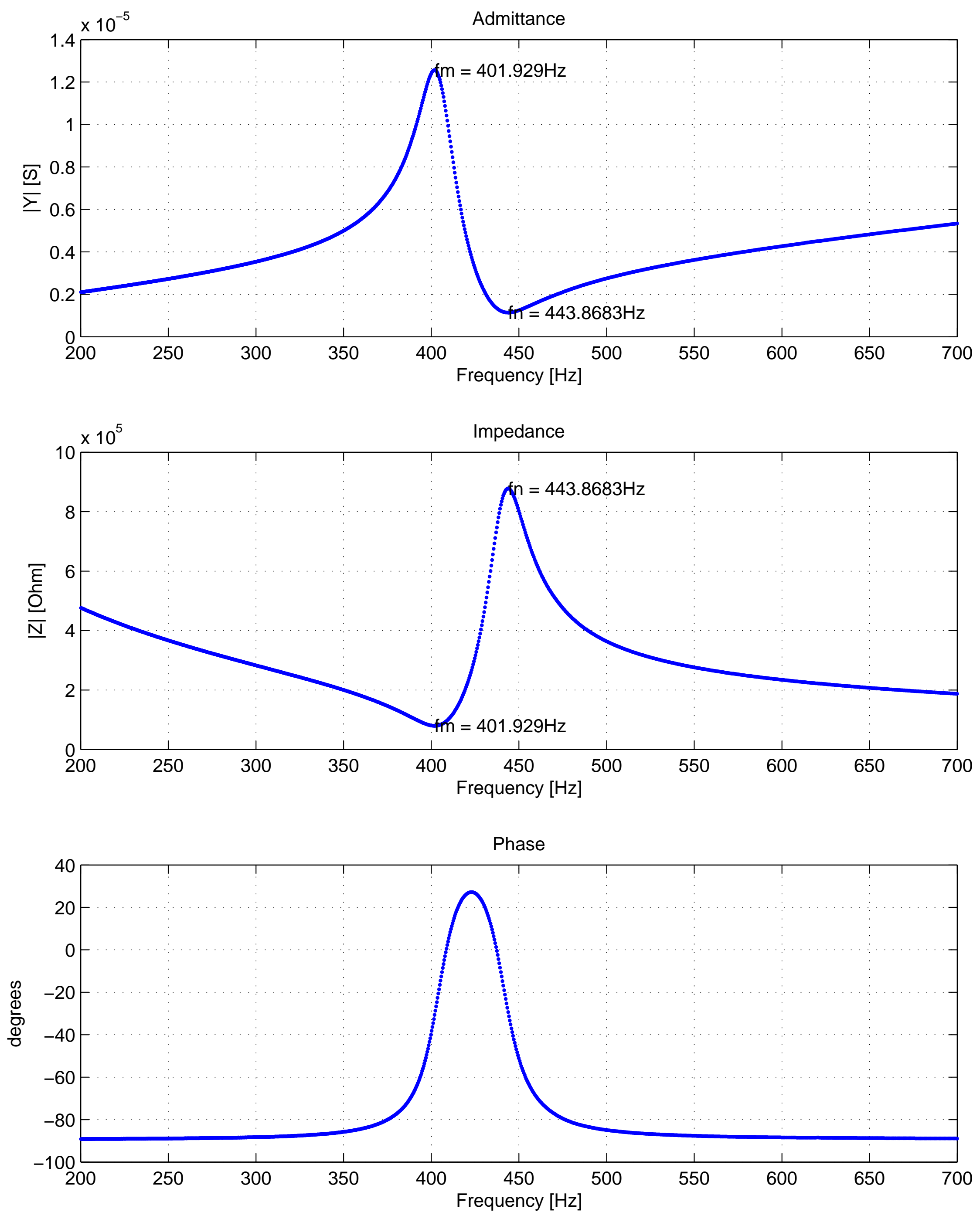

Figure 4.9: Bode plot for admittance and impedance without shunt capacitance.

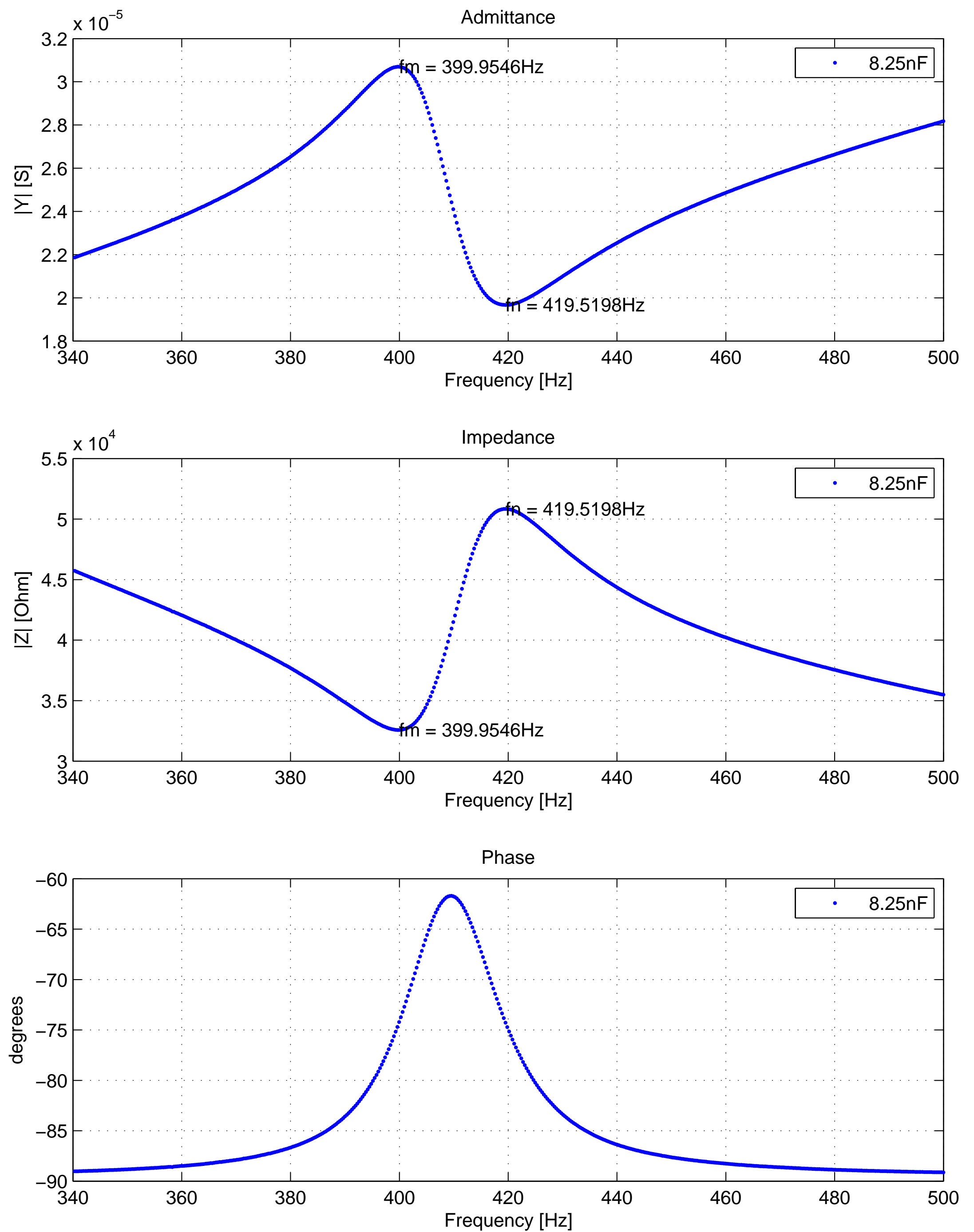

Figure 4.10: Bode plot for admittance and impedance with $C_s = 8.25nF$.

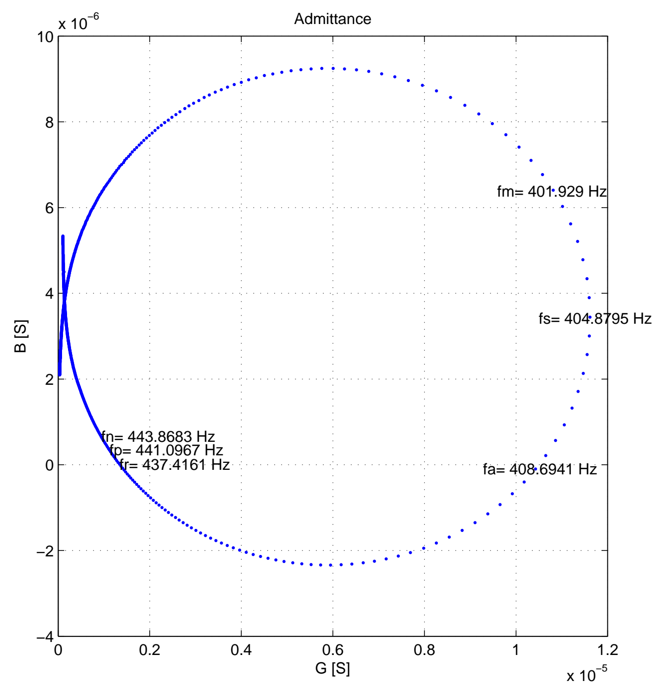

Figure 4.11: Nyquist plot of Admittance without shunt capacitance.

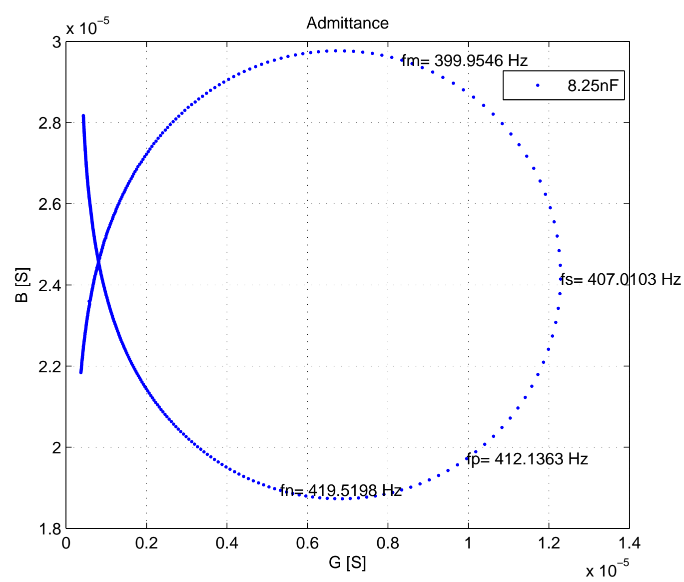

Figure 4.12: Nyquist plot of Admittance with $C_s = 8.25nF$.

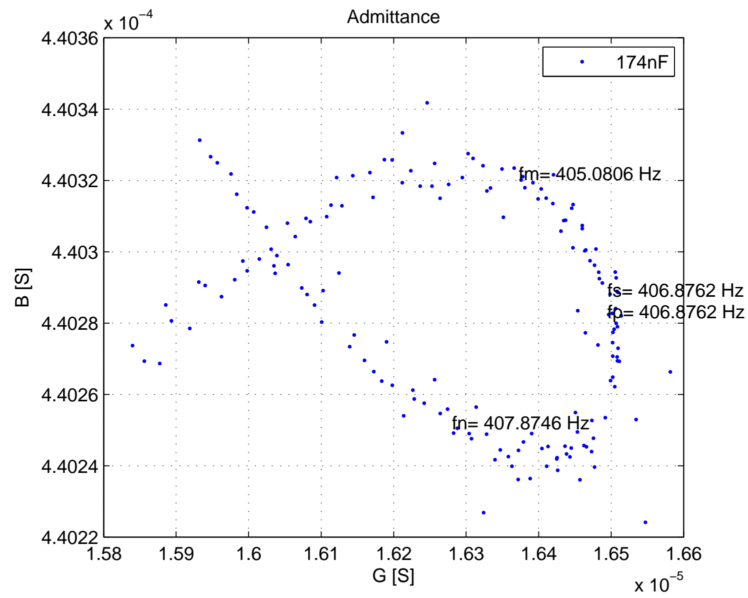

Figure 4.13: Nyquist plot of Admittance with $C_s = 174nF$.

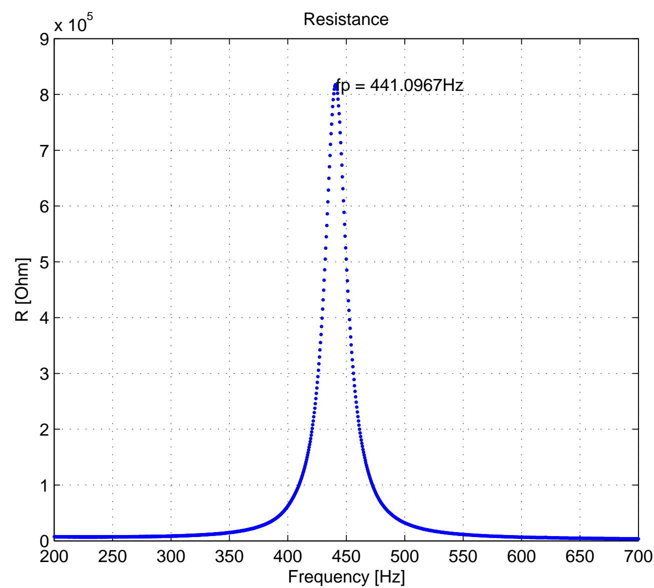

Figure 4.14: Resistance as function of the frequency without shunt capacitance.

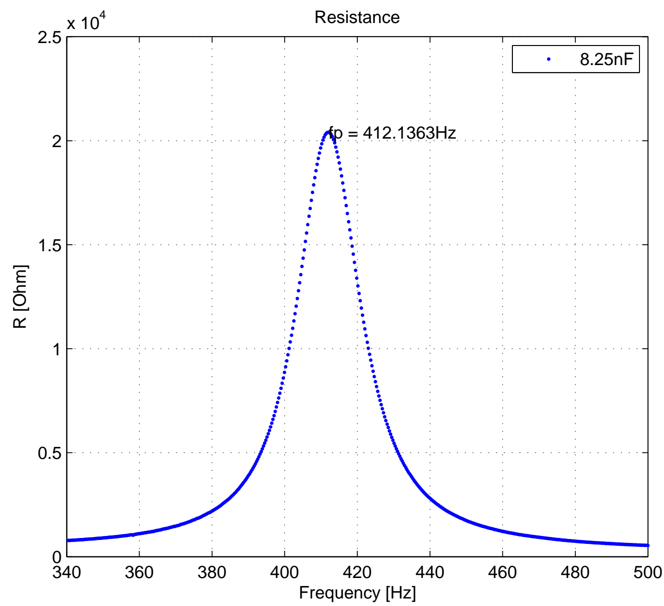

Figure 4.15: Resistance as function of the frequency with $C_s = 8.25nF$.

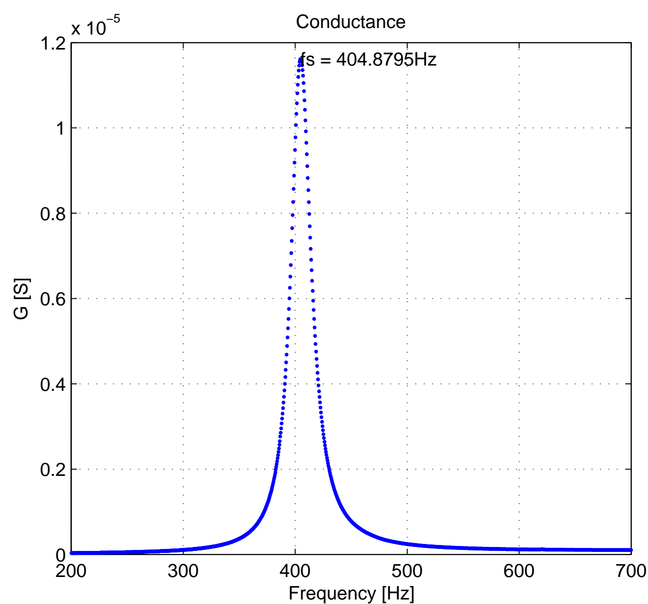

Figure 4.16: Conductance as function of the frequency without shunt capacitance.

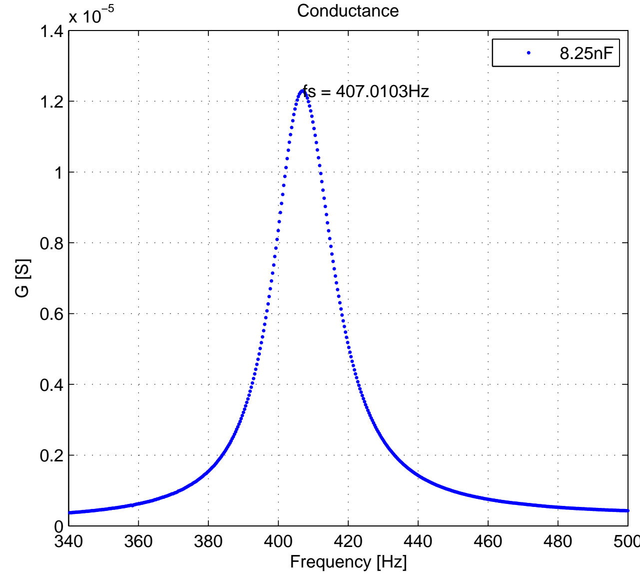

Figure 4.17: Conductance as function of the frequency with $C_s = 8.25nF$.

4.4 Electrical parameters

A *curve fitting* [30] of the electrical impedance (applicable also on the admittance) was introduced by using the *Nelder-Mead algorithm* [31] for minimizing the difference between the real measurment and the electrical model, developed by Butterworth-van Dyke.

First of all, each electrical parameter is pre-calculated with equations written in the previous section, Fig. 4.18. After that, their values are given as input of the fitting algorithm, which is applied on the first configuration without shunt capacitance, Fig. 4.19.

The eletrical parameters obtained are:

$$C_m = 246.25\,pF; \quad C_p = 1.34\,nF \quad L_m = 625.97\,H; \quad R_m = 89.84\,k\Omega; \tag{4.17}$$

Then, the *quality factor* of the whole structure is:

$$Q_m = \frac{1}{R_m}\sqrt{\frac{L_m}{C_m}} = 17.75 \tag{4.18}$$

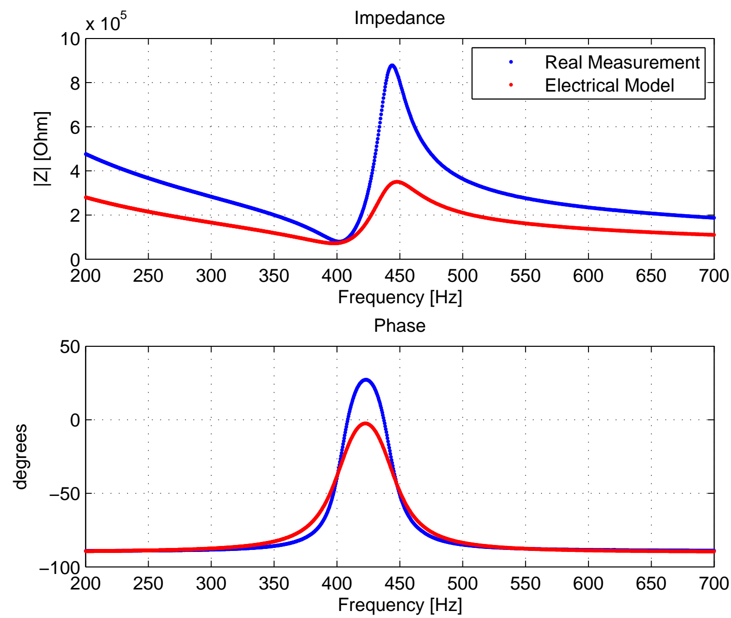

Figure 4.18: Electric model and real measurement compared before the curve fitting.

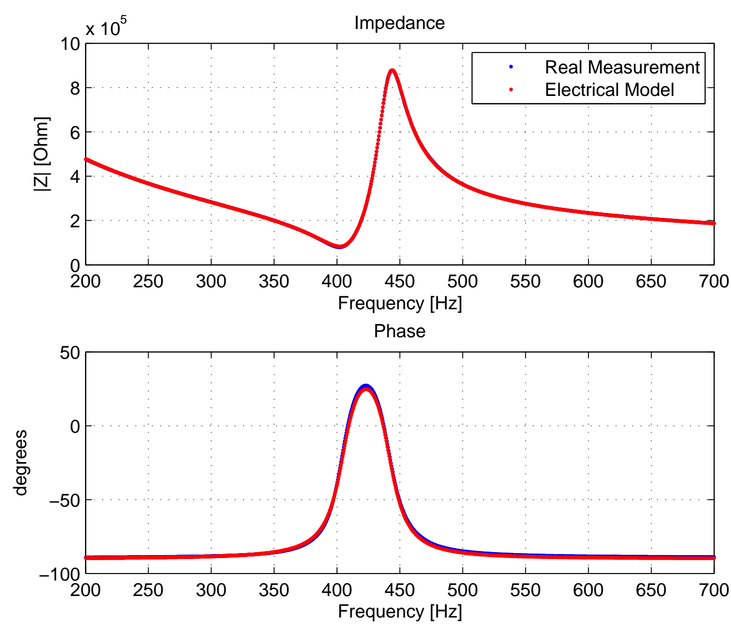

Figure 4.19: Electric model and real measurement totally matched after the curve fitting.

Chapter 5

Self-tuning piezoelectric vibration

5.1 Test stand for tuning the resonance frequency

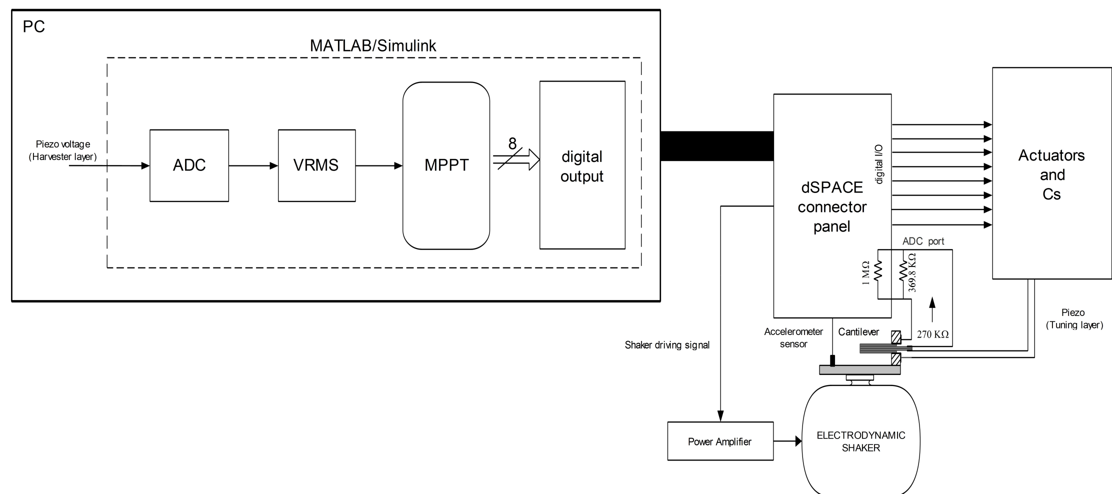

Figure 5.1: Test stand for tuning the resonance frequency with the environmental vibration.

Basically, the test stand in Fig. 5.1, is based on the same equipment shown previously. However, the focus of this thesis is on the *algorithm* used for matching the resonance frequency of the cantilever beam with the environmental vibration. The piezoelectric voltage of the harvester layer is connected to the ADC port of the dSPACE control panel, as input of the whole system.

Subsequently, an MPPT algorithm has been developed by following the RMS value of the piezo. Hence, an 8 bit digital output is constantly updated for driving the actuators and changing the stiffness of the cantilever beam.

5.2 Actuators and shunt capacitance

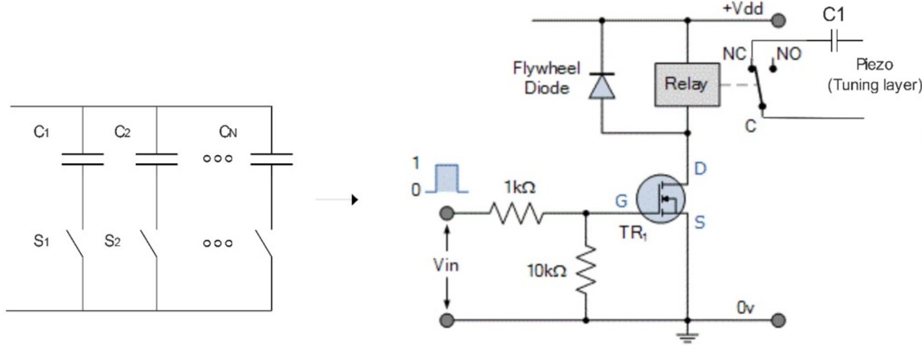

Figure 5.2: Hardware design for the piezoelectric tuning, by using relays and shunt capacitance. The picture on the right shows only the first stadium (C_1 and S_1) of the binary capacitance array, represented in the picture on the left.

The load is applied on the tuning layer by using a binary capacitance array [32]. It is based on N capacitance which are connected in parallel to the piezoelectric material with controlled switches.

Typically, in Energy Harvesting applications, where the power consumption is one of the most important goal to achieve, the switches are supposed to be implemented with MOSFETs with low parasitic capacitance and channel resistance. However, in order to evaluate the performance of the MPPT Algorithm, for the first set up, relays in the common configuration, shown in Fig. 5.2, were used in order to obtain an almost ideal electric contact. The values of the capacitance array are chosen as function of the results obtained in Chapter 3, Fig. 3.11.

In particular, the linear part of the curve has the following range of capacitance:

$$75\ pF < C_s < 65.6\ nF \tag{5.1}$$

Hence, the capacitance were fixed inside the limits over illustrated and the array is composed with $N = 8\ bit$ which features are:

$$C_1 = 100\ pF \ldots C_8 = 12.8\ nF \tag{5.2}$$

$$C_{max} = \sum_{0}^{N-1} 2^i\ C_1 = \sum_{0}^{7} 2^i\ 100\ pF = 24.78\ nF \tag{5.3}$$

- $\mathbf{C_1 = \Delta C_s}$: step-size of the shunt capacitance
- $\mathbf{C_{max}}$: maximum capacitance obtained with the 8 bit array used in my thesis

5.3 MPPT Algorithm: Perturb and Observe (P&O)

Fig. 5.6 shows the MATLAB Simulink software implemented for this task. The ADC port has a dynamic range of $\pm 10V$ and due to the attenuation factor of 10 there is a gain block of the same value.

The system provides a sine wave excitation on the top of the electrodynamic shaker. Then, also the piezoelectric voltage is sinusoidal and its root mean square value is evaluated, in order to use it as input of the maximum power point tracking. The implementation of the quadratic mean is made through a computationally efficient moving average, which is typically used in microcontrollers [33]. The mathematical formulation is given by the following equation:

$$MA^*_{(i)} = MA^*_{(i-1)} + X_{(i)} - \frac{MA^*_{(i-1)}}{N} \quad where \quad MA_{(i)} = \frac{MA^*_{(i)}}{N} \tag{5.4}$$

- $\mathbf{X_{(i)}}$: current sample
- $\mathbf{MA_{(i)}}$: moving average
- **N**: number of samples

By adjusting the number of samples N there is a trade-off between the RMS voltage accuracy and the time used to calculate it. The real time control system has a loop frequency fixed at 7.5 KHz, for this reason, the time necessary for evaluating the moving average is:

$$t_{MA} = N\frac{1}{7500Hz} = \frac{3000\ samples}{7500\ Hz} = 0.4\ sec \tag{5.5}$$

Each update of the moving average is ready after t_{MA} seconds. Thus, the MPPT algorithm has to change the output capacitance through the actuators with a time $t > t_{MA}$.

The heart of the whole system is represented in the state machine of Fig. 5.5, which implements the *Perturb and Observe* algorithm [34] shown in Fig. 5.4.

First of all, the shunt capacitance $C_{max}/2$ is chosen as starting point in the middle of the binary capacitance array. In this manner, the algorithm can decide to increase its value or decrease it as function of the piezoelectric response.

Then, the piezoelectric RMS voltage is evaluated and compared with the previous one. If the condition is *true*, the effect is an increment of the shunt capacitance in parallel of the tuning layer. Instead, when the condition is *false* the minimum capacitance step-size (ΔC_s) is inverted in order to change the direction. Finally, all values are stored and after one second the loop starts again to calculate the quadratic mean of the current voltage.

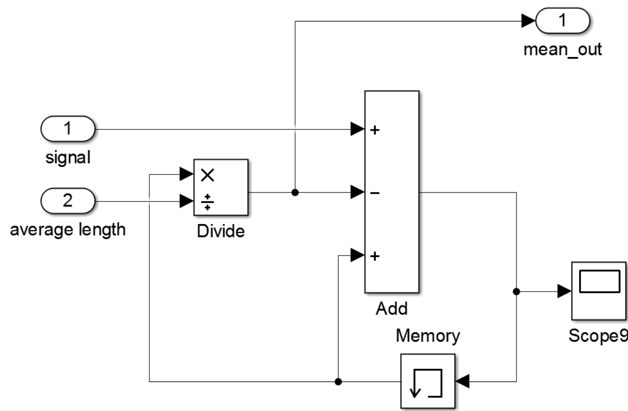

Figure 5.3: Moving average in MATLAB Simulink.

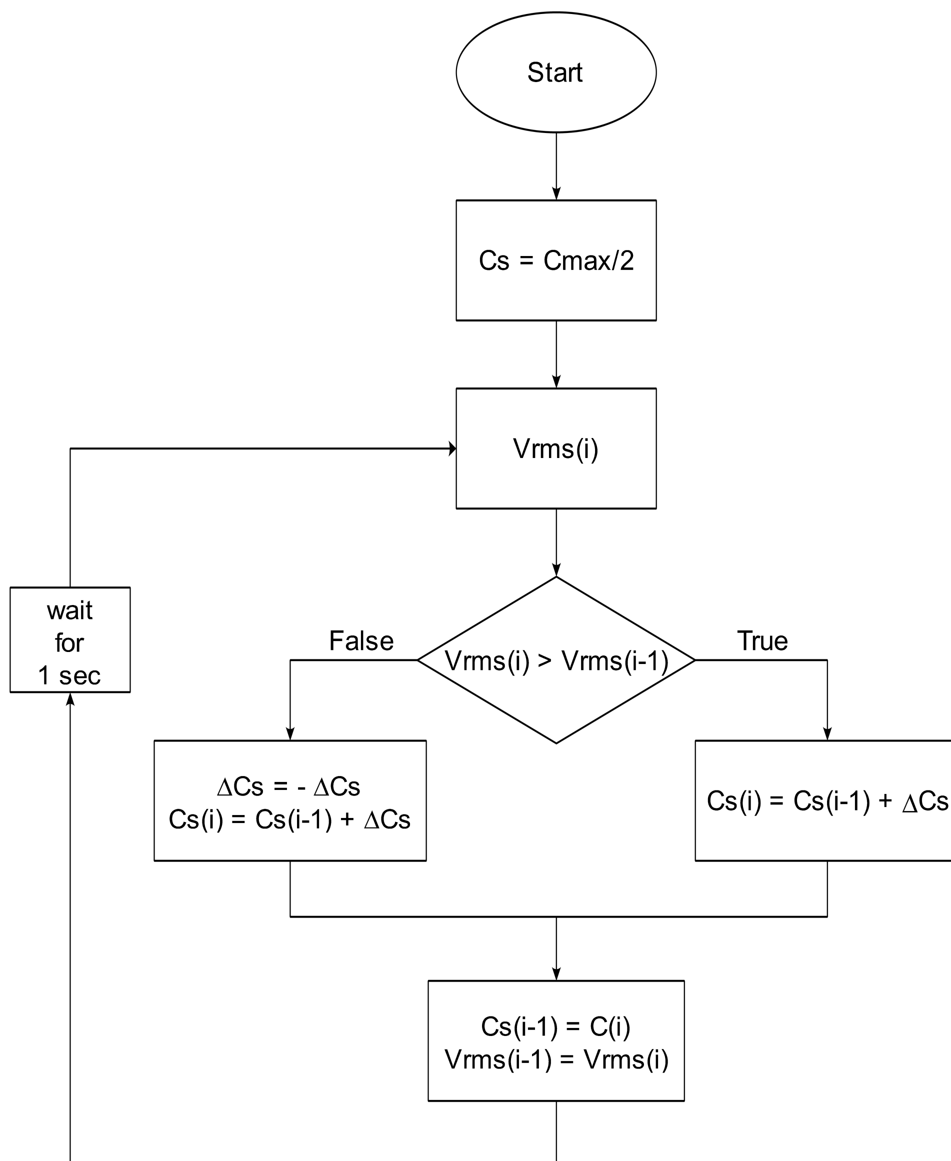

Figure 5.4: Flowchart MPPT algorithm: Pertub and Observe ($P\&O$).

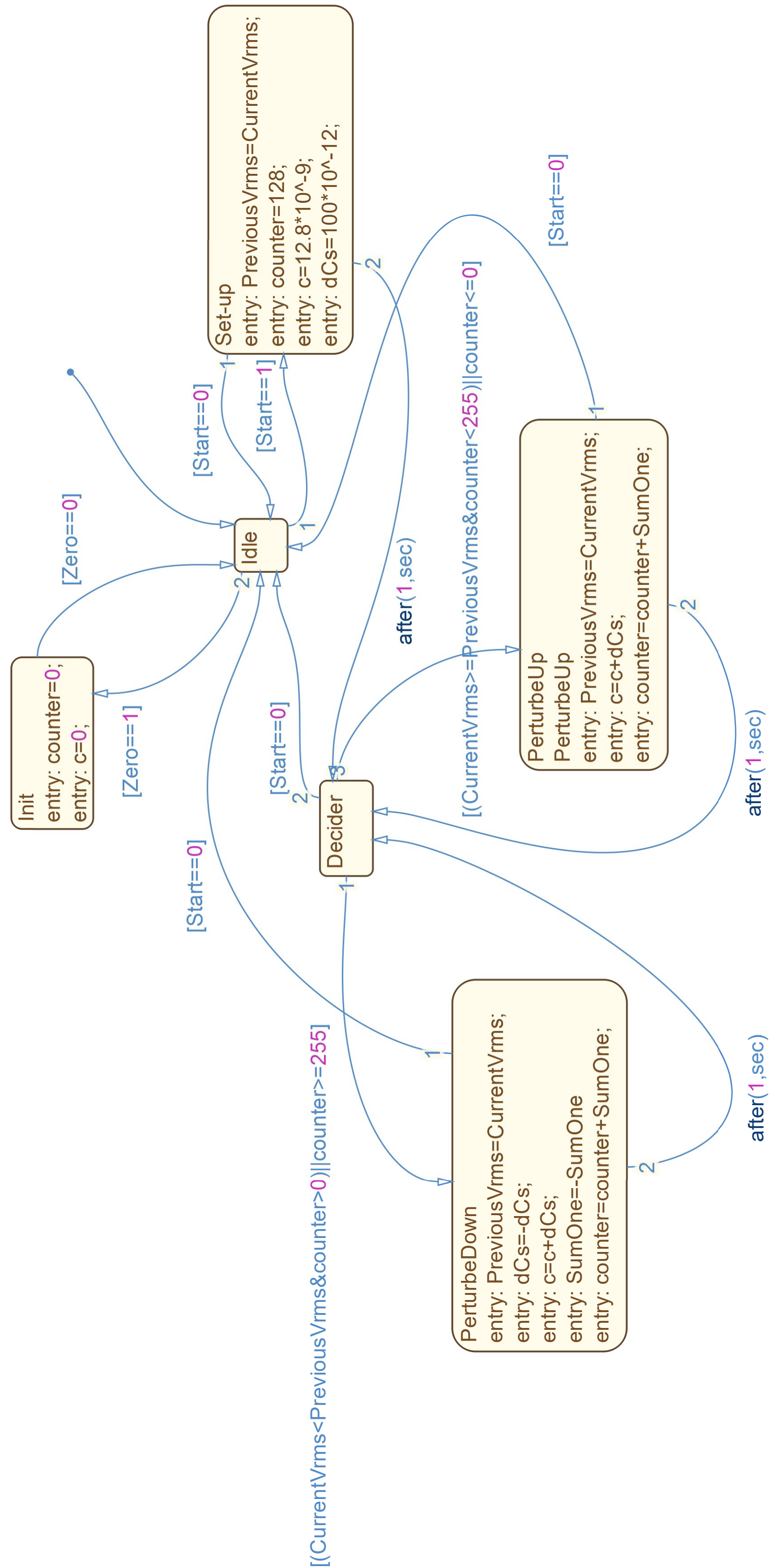

Figure 5.5: State machine MPPT algorithm Perturb & Observe (P&O)

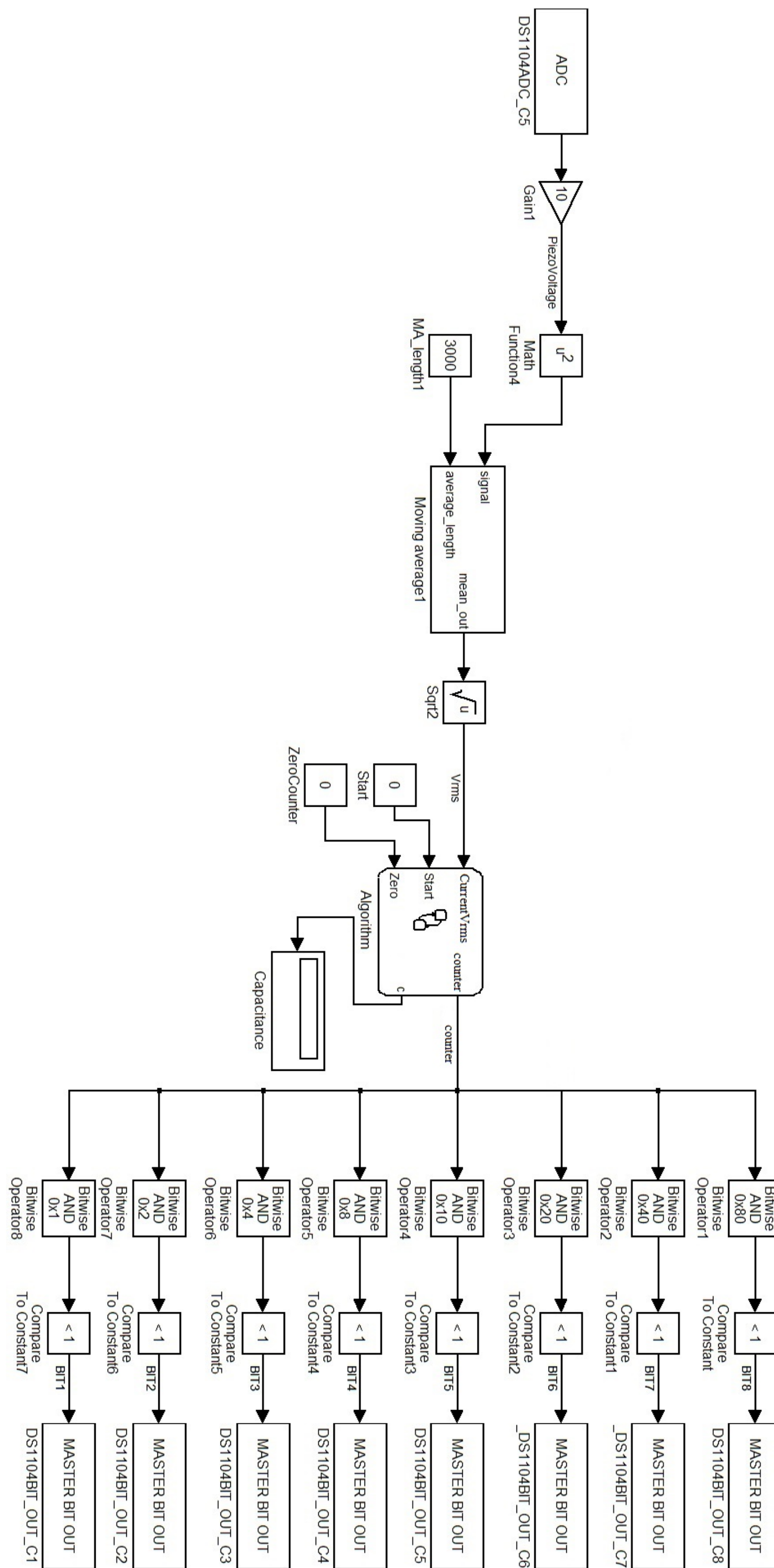

Figure 5.6: Matlab Simulink algorithm

5.4 Results and considerations

The effectiveness of the MPPT algorithm is evaluated with different measurements, performed on the tuning layer output power, in three kinds of situation:

- frequency step
- up frequency sweep
- down frequency sweep

In the first case, Fig. 5.8, frequency steps are applied on the top of the shaker as proof that the algorithm works. In fact, when it is running ($Start = 1$) for each frequency used, the output power rises up to the maximum power by adjusting the capacitance load on the tuning layer. The time necessary in order to maximize the power depends on the velocity of the MPPT algorithm. In my thesis, the system works all the time for achieving this goal and it updates the output actuators each second.

However, as future step, for energy harvesting purpose, it is necessary to save the energy, for example, by starting the algorithm only when the output power is significantly smaller than before in a certain percentage. In addition, a detailed low-level implementation with very low consumption has also to be devised.

The effect of the algorithm on the output power, compared with a solution without self-tuning, is better shown in Fig. 5.9 and in Fig. 5.10. In both pictures, a frequency sweep is generated for a continuous tuning of the resonance frequency with the environmental vibration. In particular, a tuning ratio over 10% is found when the MPPT algorithm is ON, which brings the piezoelectric elements to produce the maximum power.

However, the approach to use the quadratic mean of the piezoelectric voltage, as input of the Perturb and Observe algorithm, is only suitable when a sinusoidal waveform is reproduced on the shaker. In fact, a lot of problems come out when this system has to work with a real acceleration data where just the amplitude changes (and mantain the frequency) or signals with more than one frequency component. For this reason, another approach is necessary.

The *phase shift approach* was investigated for following the vibration frequency.

Basically it is based on the phase shift between the acceleration signal and the piezoelectric voltage, which solution is object of the next and last chapter.

Figure 5.7: Control Desk interface used for driving the MPPT algorithm

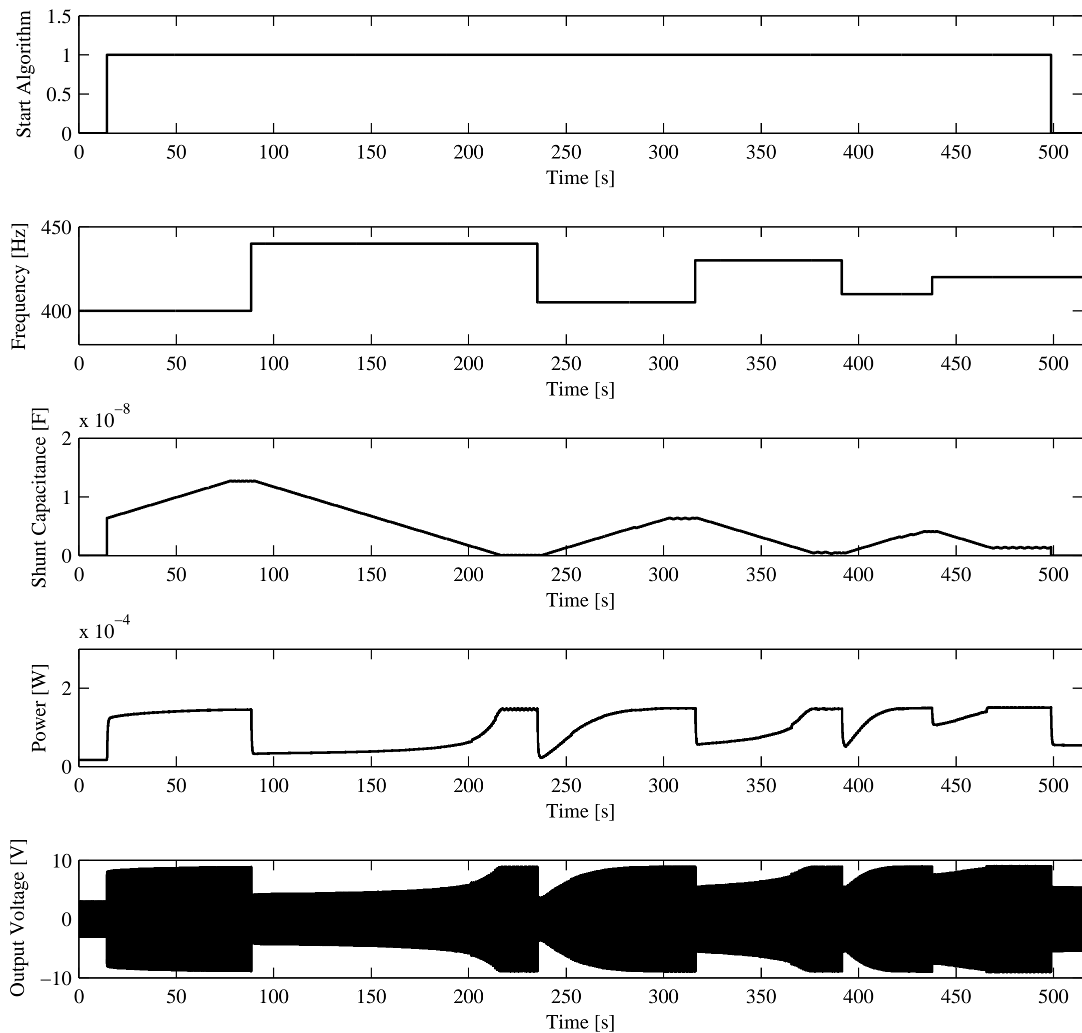

Figure 5.8: Measurement of the tuning layer output power, with frequency step, while the MPPT Algorithm is ON.

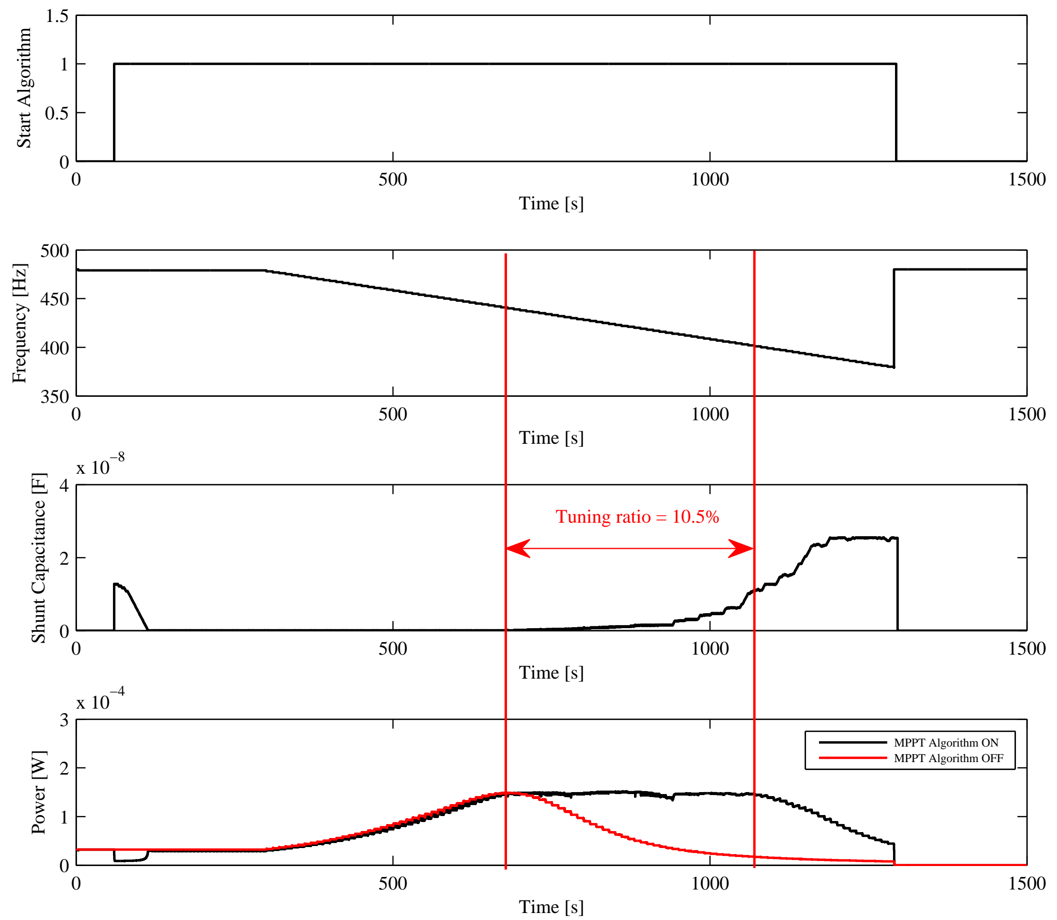

Figure 5.9: Measurement of the tuning layer output power with and without MPPT algorithm, during a down frequency sweep.

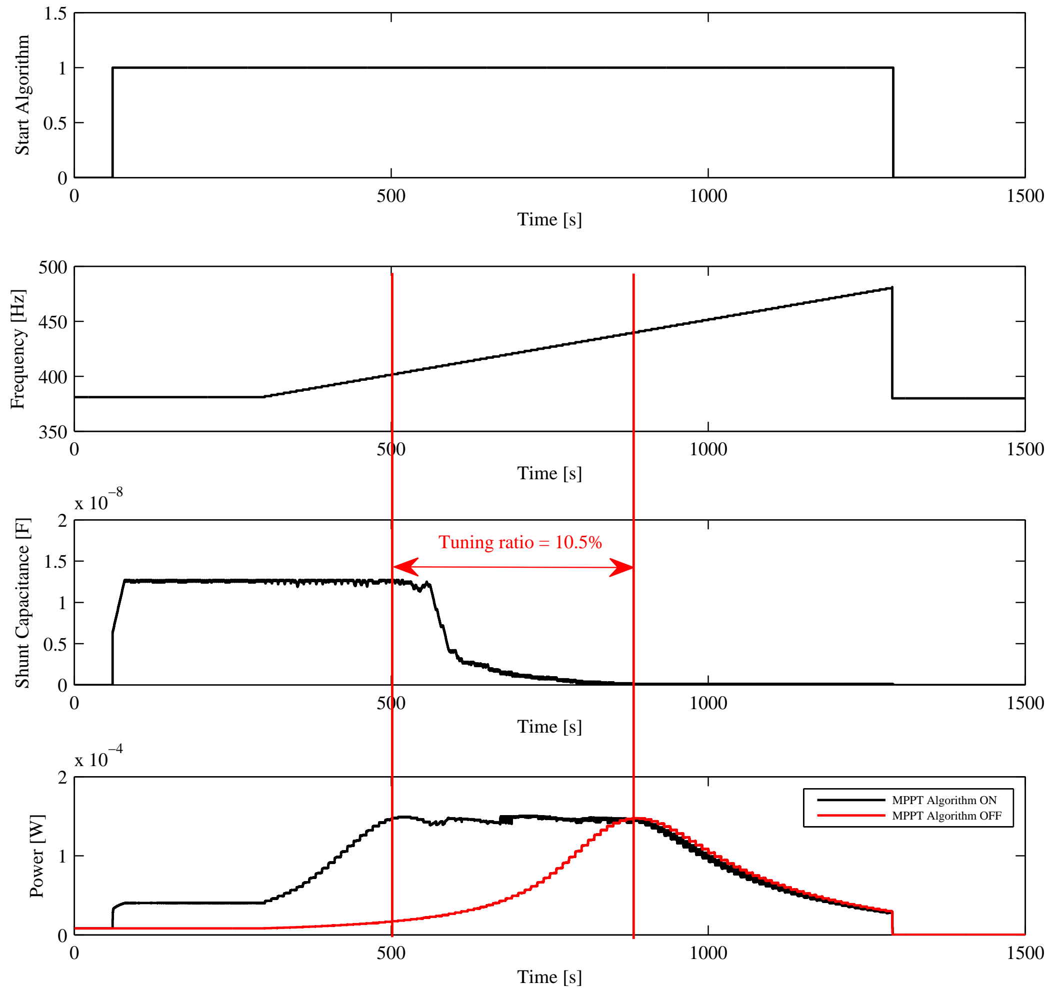

Figure 5.10: Measurement of the Output power with and without MPPT algorithm, during an up frequency sweep.

Chapter 6

Phase Shift approach

6.1 Sinusoidal Excitation

An efficient self-tuning technique for piezoelectric generators, should be independent from the amplitude of the environmental excitation, besides its frequency changing with respect to the resonance frequency. Thus, the method based on the phase shift information among the acceleration data of the base motion and the beam deflection, is suitable to achieve this goal [35].

The system SDOF [24] studied in this thesis, can be perturbed by applying a force on the base of the harvester, $f(t) = -m\ddot{y}(t)$, where m is the beam mass and $\ddot{y}(t)$ the external acceleration.

Now, the equation of motion can be easily extrapolated from Fig. 1.10 (Chapter 1):

$$\begin{aligned} m(\ddot{x}(t) + \ddot{y}(t)) + d_m\dot{x}(t) + kx(t) = 0 \\ m\ddot{x}(t) + d_m\dot{x}(t) + kx(t) = -m\ddot{y}(t) \\ \ddot{x}(t) + 2\xi\omega_n\dot{x}(t) + \omega_n^2 x(t) = -\ddot{y}(t) \end{aligned} \quad (6.1)$$

- $\mathbf{d_m}$: equivalent mechanical damping
- **m**: effective mass of the cantilever beam
- **k**: mechanical stiffness of the cantilever beam
- $\omega_\mathbf{n}$: natural frequency
- $\xi = \dfrac{\mathbf{d_m}}{\mathbf{2m}\omega_\mathbf{n}}$ damping ratio

Eq. 6.1 shows that the system is independent from the mass m and its response depends on the mechanical damping besides the natural frequency.

I suppose to apply a sinusoidal excitation to the electrodynamic shaker, then, the base displacement can be written as follows:

$$y(t) = \overline{Y}\cos(\omega t) \tag{6.2}$$

Hence, the acceleration and the force related to the base are:

$$\ddot{y}(t) = -\overline{Y}\omega^2\cos(\omega t) \tag{6.3}$$

$$f(t) = m\overline{Y}\omega^2\cos(\omega t) \tag{6.4}$$

If the acceleration is persistent, the piezoelectric response will have the same frequency w at steady-state. For this reason, the beam deflection is:

$$x(t) = \overline{X}\cos(\omega t + \theta) \tag{6.5}$$

with $\theta =$ *phase shift between the external acceleration and the beam displacement.* Hence, by applying the trigonometric identities:

$$x(t) = \overline{X}\cos(\theta)\cos(\omega t) - \overline{X}\sin(\theta)\sin(\omega t) \tag{6.6}$$

$$a = \overline{X}\cos(\theta) \tag{6.7}$$

$$b = -\overline{X}\sin(\theta) \tag{6.8}$$

Then, the beam displacement, velocity and acceleration are respectively:

$$\begin{aligned} x(t) &= a\cos(\omega t) + b\sin(\omega t) \\ &= X(\omega)e^{+j\omega t} + X^*(\omega)e^{-j\omega t} \end{aligned} \tag{6.9}$$

$$\dot{x}(t) = j\omega X(\omega)e^{j\omega t} - j\omega X^*(\omega)e^{-j\omega t} \tag{6.10}$$

$$\ddot{x}(t) = -\omega^2 X(\omega)e^{j\omega t} - \omega^2 X^*(\omega)e^{-j\omega t} \tag{6.11}$$

The last three equations are expressed with complex exponentials by applying *Euler's formula*, which complex coefficients are: $X = A + jB$ and $X^* = A - jB$ ($a = A/2$, $b = -b/2$).

Furthermore, the coefficient $X(\omega)$ corresponds to the positive frequencies while $X^*(\omega)$ to the negative frequencies. In this manner, these coefficients can be studied separately because of their independence.

Hence, I consider only the positive solution, so, by replacing (6.9), (6.10), (6.11) and (6.3) in (6.1) we obtain the following equation that characterizes all the system:

$$\begin{aligned} \frac{X(\omega)}{Y(\omega)} &= \frac{m\omega^2}{(k - m\omega^2) + j(d_m\omega)} \\ &= \frac{\Omega^2}{(1 - \Omega^2) + j(2\xi\Omega)} \end{aligned} \tag{6.12}$$

where $\Omega = \omega/\omega_n$ is the ratio between the forcing frequency and the natural frequency.

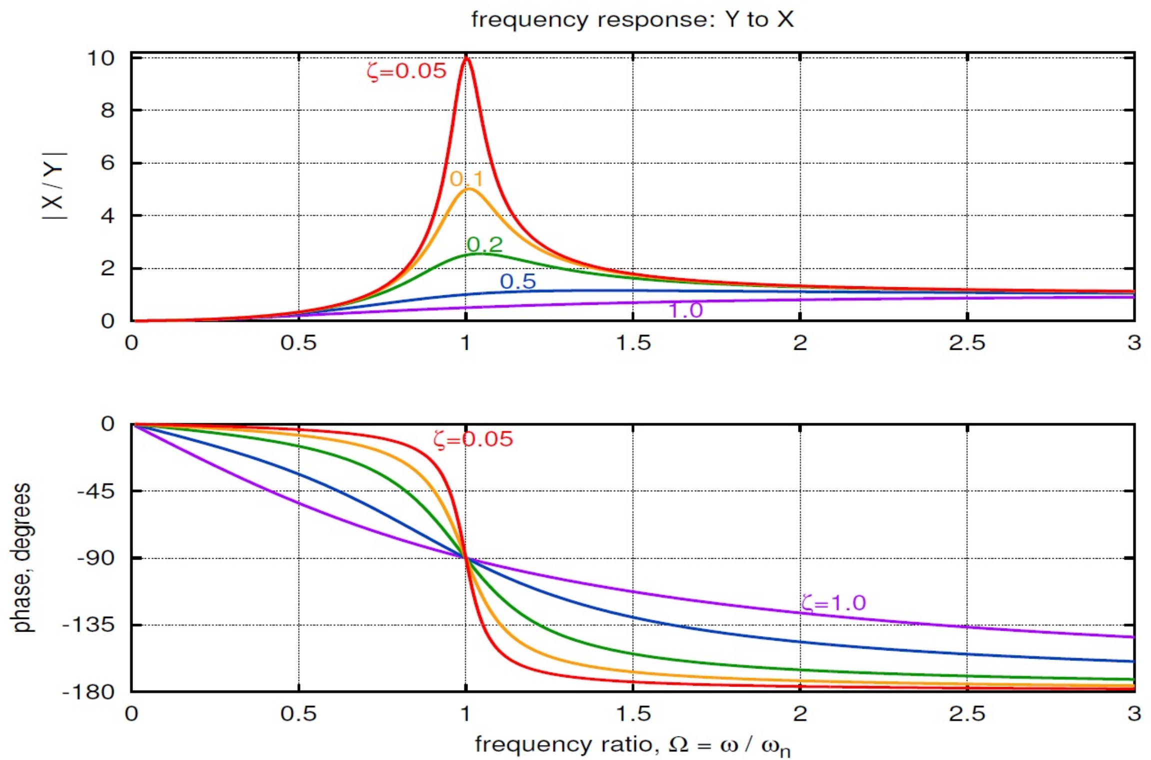

Figure 6.1: Magnitude and phase of the frequency response function, in a SDOF system, with a sinusoidal excitation [24].

Considering an *under-damped* system where the mechanical damping is positive, but less than the critical one, the phase shift between the acceleration of the base and the beam displacement has a value of -$\pi/2$ when $w = w_n$.

Vibration frequency	phase-shift [degrees]
f = 400.29 Hz	175.9
f = 445.20 Hz	98.42
f = 447.68 Hz	90.56
f = 449.45 Hz	86.1
f = 480.15 Hz	40.31
f = 550.95 Hz	16.1

Table 6.1: Phase-shift between the accelerometer signal (excitation) and the piezoelectric output voltage. The resonance frequency of the cantilever beam is $fr = 447Hz$ which is about the same frequency we have already seen in the previous chapters.

As proof of this important result, a sinusoidal excitation has been applied on the top of the electrodynamic shaker in order to evaluate the acceleration signal of the base. The voltage and the displacement generated from the piezoelectric materials are proportional with the same phase [36].

For this reason, the measurement of the cantilever displacement has been replaced with the evaluation of its output voltage, which is much easier to measure without a particular instrumentation needed to define the beam deflection. The results, collected in Tab. 6.1, show a phase shift of $\pi/2$ when the piezoelectric resonance frequency is matched with the frequency of the excitation.

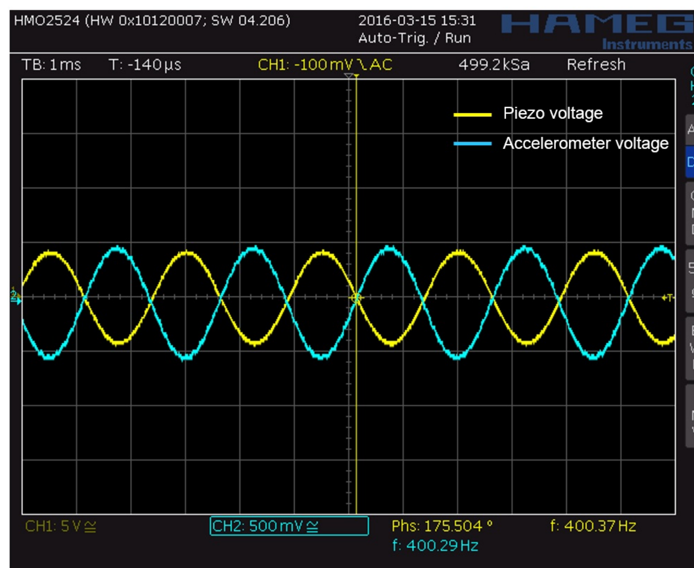

Figure 6.2: Measurement of the phase-shift between the acceleration signal applied as excitation ($f = 400.29\ Hz$) and the piezoelectric voltage.

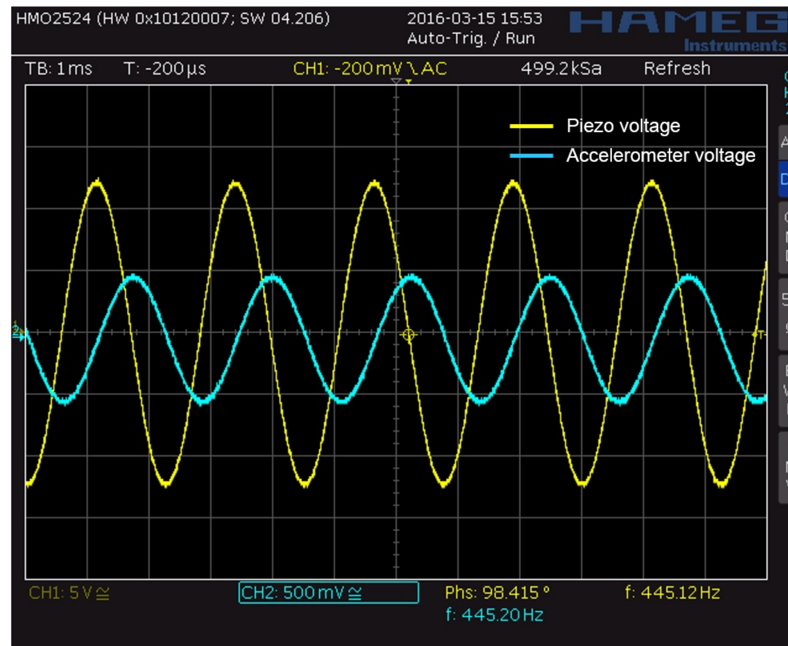

Figure 6.3: Measurement of the phase-shift between the acceleration signal applied as excitation ($f = 445.20\ Hz$) and the piezoelectric voltage.

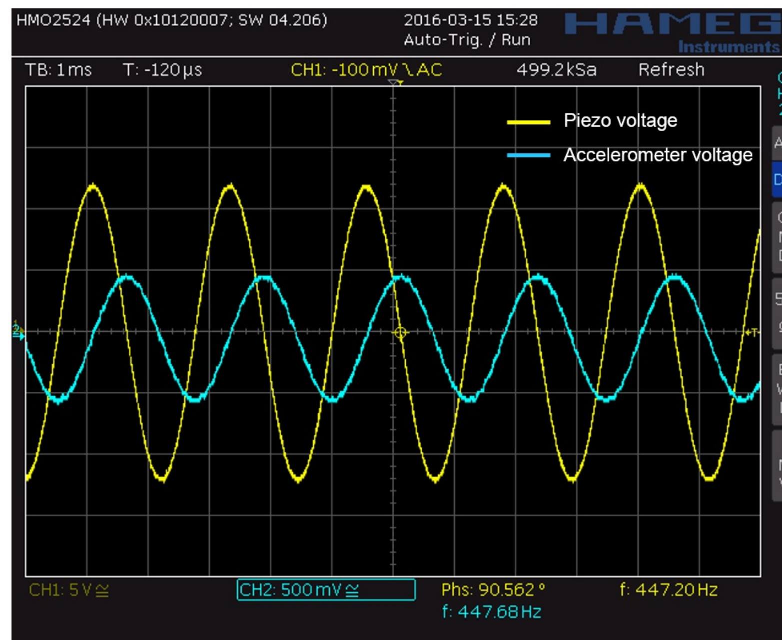

Figure 6.4: Measurement of the phase-shift between the acceleration signal applied as excitation ($f = 447.68\ Hz$) and the piezoelectric voltage.

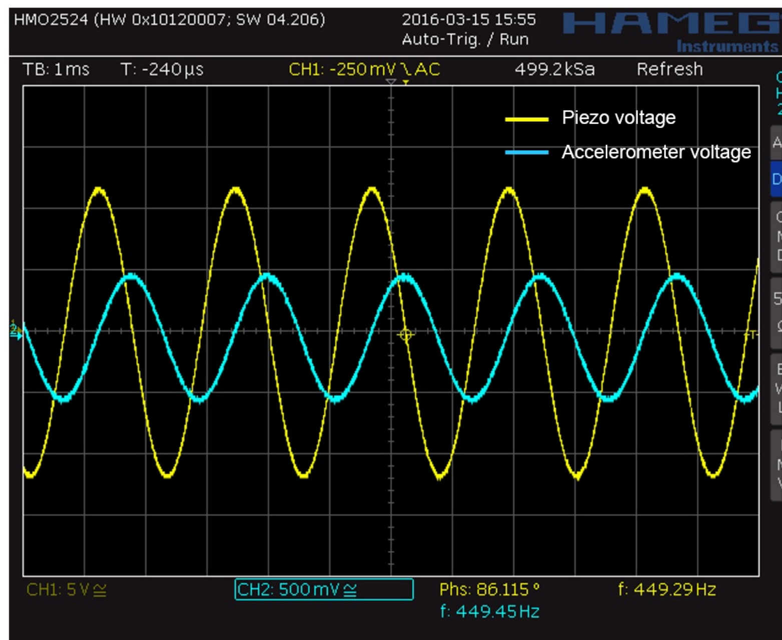

Figure 6.5: Measurement of the phase-shift between the acceleration signal applied as excitation ($f = 449.45\ Hz$) and the piezoelectric voltage.

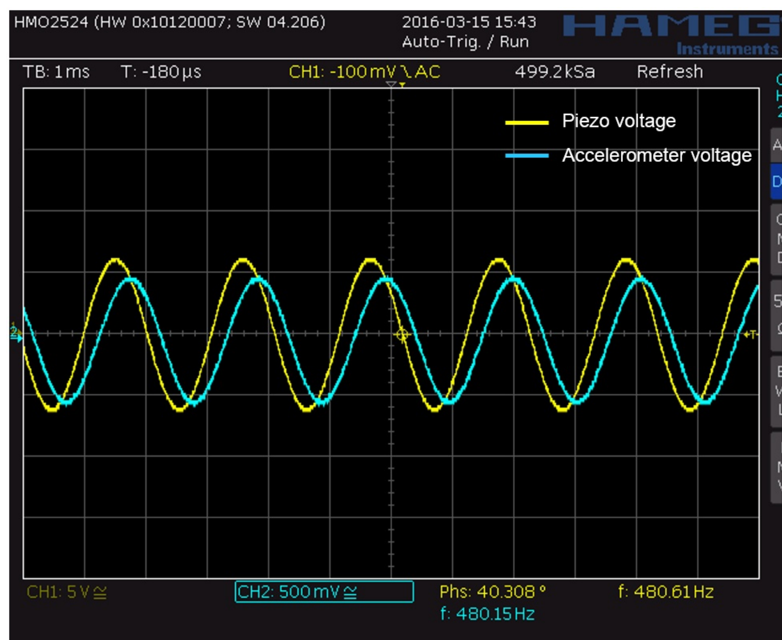

Figure 6.6: Measurement of the phase-shift between the acceleration signal applied as excitation ($f = 480.15\ Hz$) and the piezoelectric voltage.

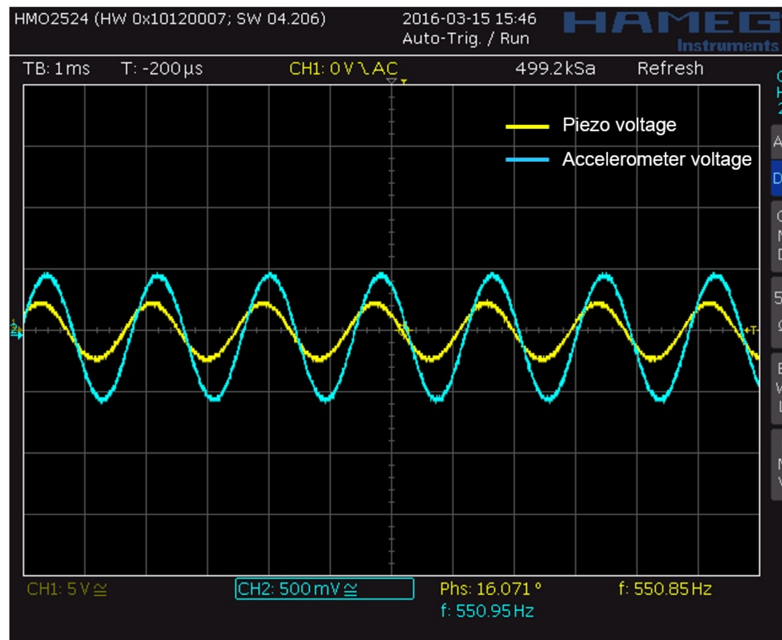

Figure 6.7: Measurement of the phase-shift between the acceleration signal applied as excitation ($f = 550.95\ Hz$) and the piezoelectric voltage.

6.2 Multisine excitation

The typical acceleration data stored from an environmental source, which could be the vibration of a train, airplane and so on, has a main component in a certain frequency, where the vibration is mostly concentrated, and secondary components at different frequencies. The meaning of a multisine excitation is to emulate a real vibration data in order to understand if the phase-shift algorithm still works. Thus, I generated on MATLAB three kinds of signals with the following features:

- **First exctiation** (Fig. 6.8a)

$$\begin{aligned} x_1(t) = 0.2\sin(2\pi 200t) + 0.3\sin(2\pi 350t) + \\ \sin(2\pi 440t) + 0.2\sin(2\pi 480t) + 0.4\sin(2\pi 300t) \end{aligned} \tag{6.13}$$

  - Main vibration frequency: $f = 440\ Hz$
  - Pizoelectric resonance frequency: $f_r = 452\ Hz$

- **Second excitation** (Fig. 6.9a)

$$\begin{aligned} x_2(t) = 0.2\sin(2\pi 200t) + 0.3\sin(2\pi 300t) + \\ \sin(2\pi 452t) + 0.2\sin(2\pi 480t) + 0.4\sin(2\pi 550t) \end{aligned} \tag{6.14}$$

  - Main vibration frequency: $f = 452\ Hz$
  - Pizoelectric resonance frequency: $f_r = 452\ Hz$

- **Third excitation** (Fig. 6.10a)

$$\begin{aligned} x_3(t) = 0.2\sin(2\pi 200t) + 0.3\sin(2\pi 400t) + \\ \sin(2\pi 550t) + 0.2\sin(2\pi 480t) + 0.4\sin(2\pi 300t) \end{aligned} \tag{6.15}$$

  - Main vibration frequency: $f = 550\ Hz$
  - Pizoelectric resonance frequency: $f_r = 452\ Hz$

Hence, the signals have been replicated on the electrodynamic shaker and the results are shown in Fig. 6.8b, Fig. 6.9b, and Fig. 6.10b where the phase shift is calculated between the whole acceleration signals ($x_1'(t)$, $x_2'(t)$, $x_3'(t)$) and the piezoelectric voltage. When the main vibration frequency is matched with the piezoelectric resonance frequency, a phase shift of $\pi/2$ is still reached.

Thus, this approach can be used as input of the MPPT algorithm, by replacing the quadratic mean of the piezoelectric voltage. The phase shift provides an useful information suitable for many scenarios in order to understand when the piezoelectric resonance frequency is tuned with the environmental vibration.

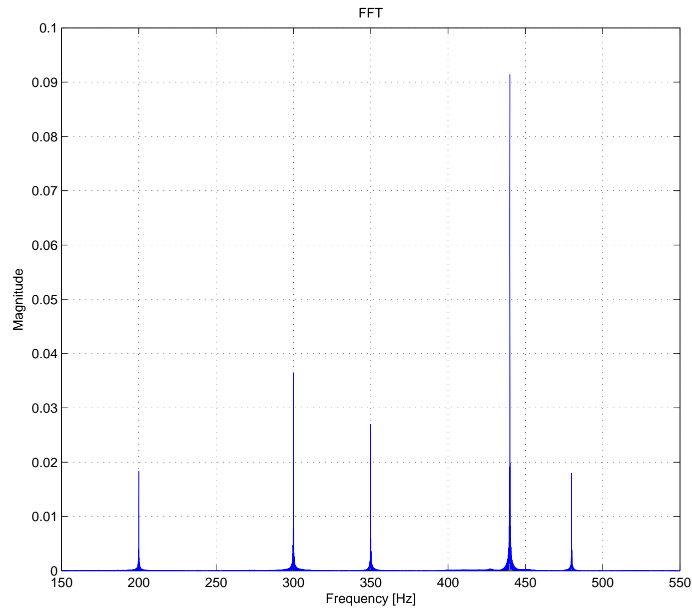

(a)

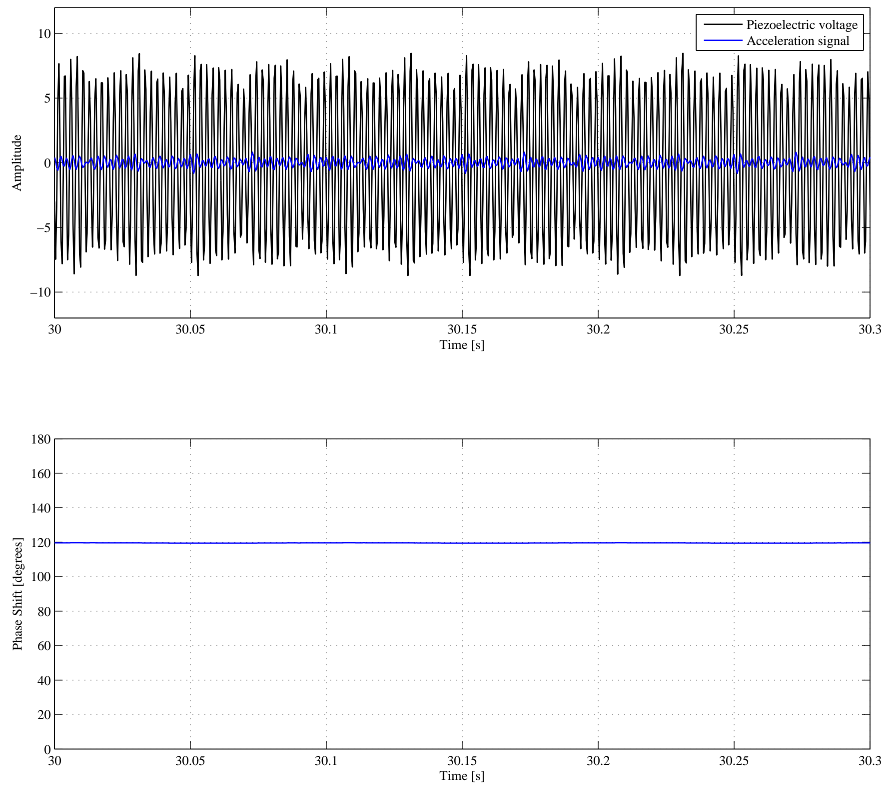

(b)

Figure 6.8: (a) FFT of the replied signal on the shaker, with the main frequency at 440 Hz (b) Phase-shift between the accelerometer signal and the piezoelectric voltage, when the vibration frequency is smaller of the resonance frequency.

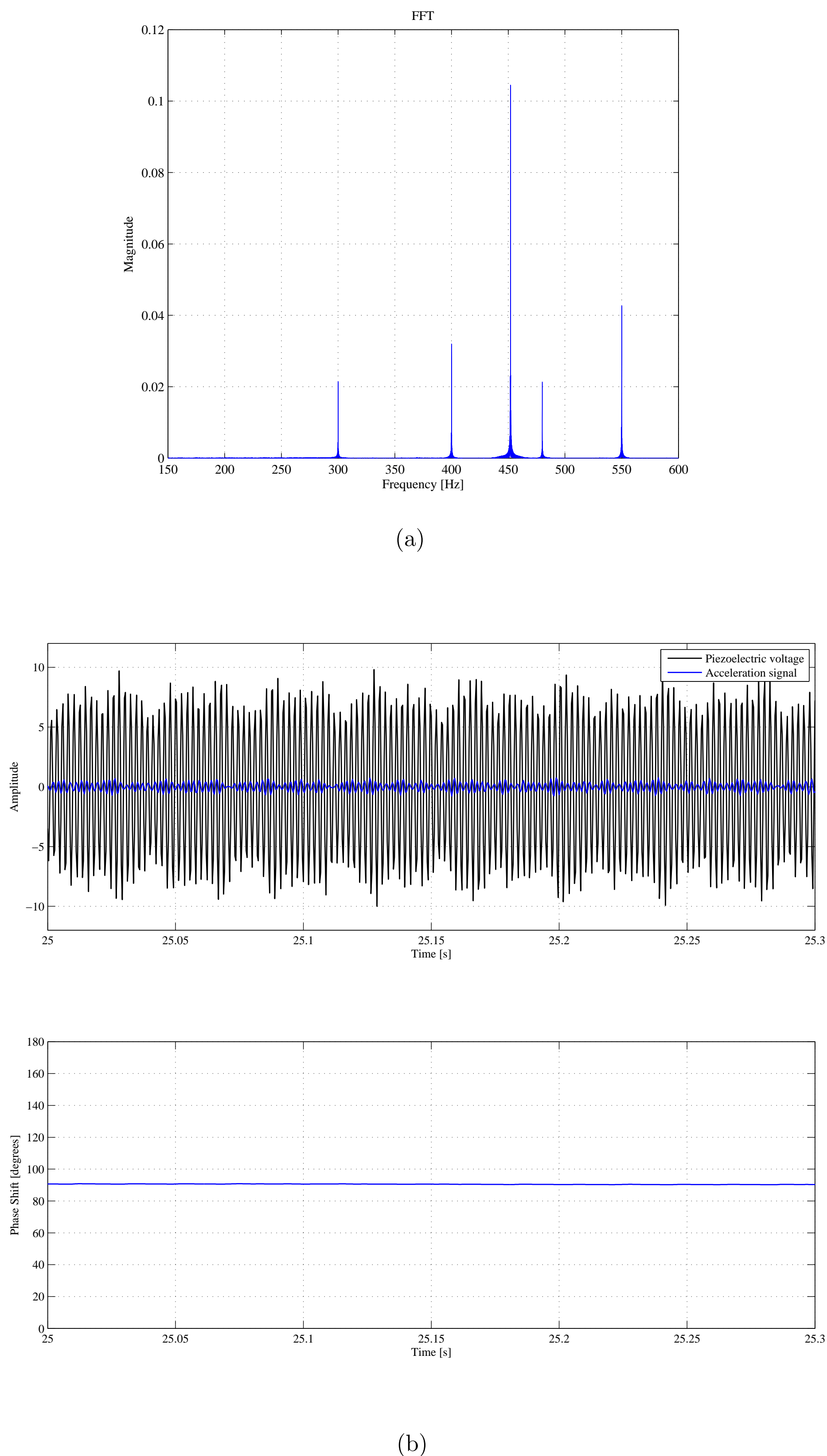

Figure 6.9: (a) FFT of the replied signal on the shaker, with the main frequency at 452 Hz (b) Phase-shift between the accelerometer signal and the piezoelectric voltage, when the vibration frequency is matched with the resonance frequency.

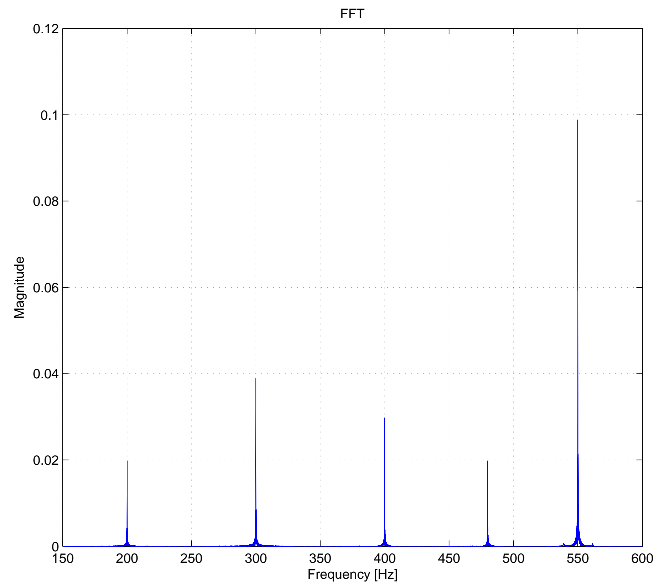

(a)

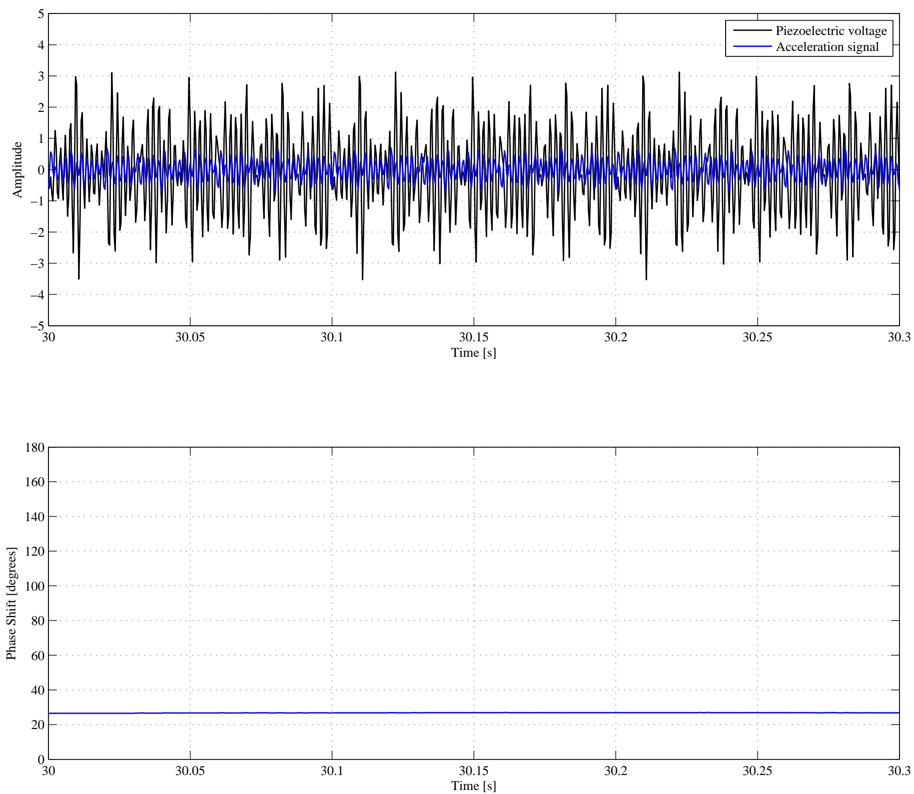

(b)

Figure 6.10: (a) FFT of the replied signal on the shaker, with the main frequency at 550 Hz (b) Phase-shift between the accelerometer signal and the piezoelectric voltage, when the vibration frequency is higher of the resonance frequency.

Chapter 7

Conclusion and future works

Starting from a single crystal piezoelectric material PZN-5.5%PT, a bimorph cantilever beam has been built with stainless steel as substrate and conductive glue, in order to bond each layer. It provides a resonance frequency around 450 Hz with a tip mass of 15 g. Hence, a tuning ratio of 10.5% has been achieved and verified with both impedance measurements and electrodynamic shaker, by adding different capacitor in parallel as load. Thus, the material PZN-5.5%PT have a higher tuning ratio than PZT piezoelectric elements, which is still at 4%.

However, adding an additional tip mass in order to reach a lower resonance frequency, needed for the most common environmental vibrations, is not a viable solution due to the brittleness of the crystals. For this reason, my suggestion is to keep the same material but with a lower thickness than 0.8 mm, used in my master thesis. In this way, the aim over mentioned is easily reachable.

The measurements with the vibration exciter show a bandwidth of 75 Hz when the tuning is made by the connection of capacitors, compared with a bandwidth of 74 Hz if a parallel and series connection are used. Therefore, the last solution should be further tested. The idea is to switch between both conditions (parallel and series) by following the maximum power.

The Perturb and Observe algorithm, using the quadratic mean of the piezoelectric voltage, has been employed and implemented on MATLAB/Simulink for an automatic tuning with capacitors. This method allows the maximum power point tracking with good results, only for sine wave excitation without changing neither amplitude nor frequency. For this reason, due to the limitations of this approach, a proof of concept using the phase shift between the accelerometer signal and the piezoelectric voltage has been successfully tested.

As future works, the MATLAB/Simulink software can be updated with the phase shift approach, which provides the tuning information of the piezoelectric resonance frequency, by using the same MPPT algorithm already implemented.

On the other hand, an autonomous system could be developed by rewriting

the same code in C language (or Assembly for the optimization) on a low power microcontroller. The solution with the quadratic mean of the piezoelectric voltage, despite its limitations, is easy to implement because it is based on a computationally efficient moving average suitable for MCU. Instead, the phase shift approach needs the calculation of the phase between two signals, which implementations has a major cost compared with the previous one. For example, by applying a cross-correlation between the signals of interest, the average time lag is obtained. Anyway, this solution is sensitive to noise and it works fine when the signal of interest is composed of a main frequency, where the amplitude is mostly distributed. Moreover, for evaluating the phase, the requirement of an accelerometer sensor, increases the power consumption of the all system, which has to be monitored.

Finally, the relays as hardware solution for switching the capacitance, are not suitable for energy harvesting purpose. The switches, in a low power implementation, are supposed to be implemented with MOSFETs with low parasitic capacitance and low channel resistance.

List of Figures

1.1 (a) Random oriented electric dipole before the polarization (b) During the polarization with a very large DC electric field. (c) After the process, the polarization is permanent. 13
1.2 Piezoelectric behaviour 13
1.3 (a) 31 mode: charge harvested in third direction and stress applied in first direction. (b) 33 mode: both charge harvested and stress are applied in third direction. 14
1.4 (a) Unimorph piezoelectric cantilever (b) Bimorph piezoelectric cantilever. 18
1.5 Bimorph piezoelectric cantilever. 19
1.6 Free-Body diagram of the system. 20
1.7 Segment of bimorph cantilever. 20
1.8 Infinitesimal part of the beam. 21
1.9 Deformation of the material before and after to apply a shear force. 21
1.10 Equivalent mechanical model (SDOF). 24
1.11 Bimorph cantilever. 25
1.12 PZN-5.5%PT piezoelecric material. 27
1.13 PI Ceramic cantilever beam with PZT piezoelectric material. 27
1.14 29
1.15 Resonance frequency as function of the capacitance ratio for PZN-5.5%PT piezoelectric materials. 30

2.1 Bimorph Cantilever 31
2.2 Resonance frequency tuning ratio as function of the thickness ratio. 33
2.3 Real bimorph cantilever. 33
2.4 A section of the structure used for clamping the cantilever beam. . 34
2.5 Top view of the Harvester. 34
2.6 Front view of the Harvester. 35

3.1 Test stand for measurement with electrodynamic shaker. 36
3.2 Main bench equipments of the whole system. 38

3.3 Real set up for measurement with electrodynamic shaker. 38
3.4 Piezoelectric damping. 39
3.5 ControlDesk inferface for measurement with electrodynamic shaker. 40
3.6 Output power of harvesting layer with and without shunt capacitance. 41
3.7 Test stand for measurement with electrodynamic shaker and fixed load. 42
3.8 Series and parallel connections of piezoelectric elements. 42
3.9 Output piezoelectric harvesting layer with and without Cs. 44
3.10 Resonance frequency tuning ratio as function of the capacitance ratio C_s/C_p by comparing both analytical model and real measurement. . 45
3.11 Tuning ratio % as function of the capacitance ratio C_s/C_p by comparing both analytical model and real measurement. 45

4.1 Piezoelectric mechanical model. 46
4.2 Piezoelectric electrical model. 47
4.3 Butterworth-van Dyke model. 48
4.4 (a) Admittance (Bode modulus and phase) diagrams of a piezoelectric material; (b) Admittance Nyquist diagram of a piezoelectric material. 49
4.5 Test stand for impedance measurement. 51
4.6 Autolab PGSTAT302N potentiostat/galvanostat. 52
4.7 Autolab Nova software: Set up for measurement 53
4.8 Real test stand for measurement. 53
4.9 Bode plot for admittance and impedance without shunt capacitance. 55
4.10 Bode plot for admittance and impedance with $C_s = 8.25nF$. 56
4.11 Nyquist plot of Admittance without shunt capacitance. 57
4.12 Nyquist plot of Admittance with $C_s = 8.25nF$. 57
4.13 Nyquist plot of Admittance with $C_s = 174nF$. 58
4.14 Resistance as function of the frequency without shunt capacitance. . 58
4.15 Resistance as function of the frequency with $C_s = 8.25nF$. 59
4.16 Conductance as function of the frequency without shunt capacitance. 59
4.17 Conductance as function of the frequency with $C_s = 8.25nF$. 60
4.18 Electric model and real measurement compared before the curve fitting. 61
4.19 Electric model and real measurement totally matched after the curve fitting. 61

5.1 Test stand for tuning the resonance frequency with the environmental vibration. 62

5.2 Hardware design for the piezoelectric tuning, by using relays and shunt capacitance. The picture on the right shows only the first stadium (C_1 and S_1) of the binary capacitance array, represented in the picture on the left. 63
5.3 Moving average in MATLAB Simulink. 65
5.4 Flowchart MPPT algorithm: Pertub and Observe ($P\&O$). 65
5.5 State machine MPPT algorithm Perturb & Observe (P&O) 66
5.6 Matlab Simulink algorithm 67
5.7 Control Desk interface used for driving the MPPT algorithm 69
5.8 Measurement of the tuning layer output power, with frequency step, while the MPPT Algorithm is ON. 69
5.9 Measurement of the tuning layer output power with and without MPPT algorithm, during a down frequency sweep. 70
5.10 Measurement of the Output power with and without MPPT algorithm, during an up frequency sweep. 71

6.1 Magnitude and phase of the frequency response function, in a SDOF system, with a sinusoidal excitation [24]. 74
6.2 Measurement of the phase-shift between the acceleration signal applied as excitation ($f = 400.29\ Hz$) and the piezoelectric voltage. 75
6.3 Measurement of the phase-shift between the acceleration signal applied as excitation ($f = 445.20\ Hz$) and the piezoelectric voltage. 76
6.4 Measurement of the phase-shift between the acceleration signal applied as excitation ($f = 447.68\ Hz$) and the piezoelectric voltage. 76
6.5 Measurement of the phase-shift between the acceleration signal applied as excitation ($f = 449.45\ Hz$) and the piezoelectric voltage. 77
6.6 Measurement of the phase-shift between the acceleration signal applied as excitation ($f = 480.15\ Hz$) and the piezoelectric voltage. 77
6.7 Measurement of the phase-shift between the acceleration signal applied as excitation ($f = 550.95\ Hz$) and the piezoelectric voltage. 78
6.8 (a) FFT of the replied signal on the shaker, with the main frequency at 440 Hz (b) Phase-shift between the accelerometer signal and the piezoelectric voltage, when the vibration frequency is smaller of the resonance frequency. 80
6.9 (a) FFT of the replied signal on the shaker, with the main frequency at 452 Hz (b) Phase-shift between the accelerometer signal and the piezoelectric voltage, when the vibration frequency is matched with the resonance frequency. 81

6.10 (a) FFT of the replied signal on the shaker, with the main frequency at 550 Hz (b) Phase-shift between the accelerometer signal and the piezoelectric voltage, when the vibration frequency is higher of the resonance frequency. 82

Bibliography

[1] Peter Spies, Loreto Mateu, Markus Pollak, *"Handbook of Energy Harvesting Power Supplies and Applications"*, 2012, Pan Stanford Publishing Pte Ltd, Available: http://www.panstanford.com/books/9789814241861.html

[2] Takuro Ikeda, *"Fundamentals of Piezoelectricity"*, 1996, New York, Oxford University Press (ISBN: 0198564600, 9780198564607)

[3] Jessy Baker, Shad Roundy and Paul Wright, *"Alternative Geometries for Increasing Power Density in Vibration Energy Scavenging for Wireless Sensor Networks"*, 2005, 3rd International Energy Conversion Engineering Conference, Available: http://dx.doi.org/10.2514/6.2005-5617

[4] *"IEEE Standard on Piezoelectricity"*, 1987, IEEE/ANSI Std. 176-1987, Available: http://dx.doi.org/10.1109/IEEESTD.1988.79638

[5] B. Ahmed Seddik, G. Despesse, S. Boisseau and E. Defay, *"Strategies for Wideband Mechanical Energy Harvester"*, 2012. Available: http://dx.doi.org/10.5772/51898

[6] Vinod R Challa, M G Prasad, Yong Shi and Frank T Fisher, *"A vibration energy Harvesting Device with bidirectional resonance frequency tunability"*, 2008, Smart Materials and Structures (Vol. 17, no. 1), Available: http://dx.doi.org/10.1088/0964-1726/17/01/015035

[7] Robert P Thornburgh and Aditi Chattopadhyay, *"Nonlinear actuation of smart composites using a coupled piezoelectric-mechanical model"*, 2001, Smart Materials and Structures (Vol. 10, no. 4), Available: http://dx.doi.org/10.1088/0964-1726/10/4/319

[8] Qing-Ming Wang, L. Eric Cross, *"Performance analysis of piezoelectric cantilever actuators"*, 1998, Ferroelectrics, 251:1, 187-213, Available: http://dx.doi.org/10.1080/00150199808229562

[9] Seon M. Han, Haym Benaroya and Timothy Wei, *"Dynamics of transversely vibrating beams using four engineering theories"*, 1999, Journal of Sound Vibration, 225(5), 935-988

[10] Tom Irvine, *"Bending frequencies of beams, rods and pipes"*, Revision S (2012), Available: http://www.vibrationdata.com/tutorials2/beam.pdf

[11] William Thomson and Peter Guthrie Tait, *"Treatise on Natural Philosophy"*, Macmillan and Co. (London), 1867

[12] A.C. Ugural and S.K. Fenster, *"Advanced Strength and Applied Elasticity"*, Prentice Hall 5th ed., 2012

[13] Mario Paz and William Leigh, *"Structural Dynamics: Theory and Computation"*, Springer 5th ed., 2006, ISBN: 978-1-4613-5098-9 [Print] 978-1-4615-0481-8 [Online]

[14] Ferdinand P. Beer, E. Russell Johnston Jr., David F Mazurek, Phillip J. Cornwell and Elliot R. Eisenberg, *"Vector Mechanics for Engineers: Statics and Dynamics"*, McGrawHill 9th ed., 2009

[15] PZN-5.5%PT single crystal piezoelectric material, Microfine Technologies Ltd (Singapore), Technical datasheet: http://www.microfine-piezo.com/files/1300852210906.pdf

[16] P-876 DuraAct Patch Transducer, PI Ceramic, Available: http://www.piceramic.com/product-detail-page/p-876-101790.html

[17] Rui Zhang, Bei Jiang, Wenwu Cao, *"Superior d^*_{32} and k^*_{32} coefficients in $0.955Pb(Zn_{1/3}Nb_{2/3})O_3 - 0.0045PbTiO_3$ and $0.92Pb(Zn_{1/3}Nb_{2/3})O_3 - 0.08PbTiO_3$ single crystal poled along [011]"*, 2004, Journal of Physics and Chemistry of Solids (Volume: 65, Issue: 6, Pages: 1083-1086), Available: http://dx.doi.org/10.1016/j.jpcs.2003.10.072

[18] Metin Sitti, Domenico Campolo, Joseph Yan, Ronald S. Fearing, Tao Su, David Taylor, Timothy D. Sands, *"Development of PZT and PZN-PT Based Unimorph Actuators for Micromechanical Flapping Mechanisms"*, 2001, ICRA IEEE International Conference on Robotics and Automation

[19] Spring steel strip, Gutekunst Stahlverformung KG, Available: http://www.gutekunst-kg.de/en/products/spring-steel-strip.html

[20] Conductive Epoxy glue CW2400, Chemtronics, Technical datasheet: https://www.chemtronics.com/descriptions/document/Cw2400tds.pdf

[21] dSPACE DS1104 R&D Controller Board, Technical information: https://www.dspace.com/shared/data/pdf/2016/dSPACE_DS1104_Catalog2016_E.pdf

[22] dSPACE, *"Hardware Installation and Configuration for DS1104 and CP1104/CLP1104 Connector Panels"*, 2004, Available: https://nees.org/data/download/NEES-2012-1123/Documentation/DS1104_config.pdf

[23] Nicanor Quijano and Kevin Passino, *"A Tutorial Introduction to Control System Development and implementation with dSPACE"*, 2002, Available: http://www2.ece.ohio-state.edu/~passino/dSPACEtutorial.doc.pdf

[24] Henri P. Gavin, *"Vibrations of Single Degree of Freedom Systems"*, 2014, Available: http://people.duke.edu/~hpgavin/cee541/sdof-dyn.pdf

[25] Jens Twiefel, Björn Richter, Tobias Hemsel and Jörg Wallaschek, *"Model based design of Piezoelectric Energy Harvesting Systems"*, 2006, Proceedings SPIE 6169, Smart Structures and Materials 2006: Damping and Isolation, Available: http://dx.doi.org/10.1117/12.658623

[26] K. S. Van Dyke, *"The Piezo-Electric Resonator and its Equivalent Network"*, 1928, Proceedings of the Institute of Radio Engineers (Volume:16 , Issue: 6, Pages: 742 - 764), Available: http://dx.doi.org/10.1109/JRPROC.1928.221466

[27] IEEE Std. No. 177-1966, *"Standard Definitions and Methods of Measurement for Piezoelectric Vibrators"*, 1966, Sponsored by: Ultrasonics, Ferroelectrics and Frequency Control Society, Available: http://dx.doi.org/10.1109/IEEESTD.1966.120168

[28] Metrohm Autolab Nova Software, *"Impedance Spectroscopy Tutorial"*, Available: http://www.ecochemie.nl/download/NovaTutorials/Impedance_measurements_tutorial.pdf

[29] Metrohm Autolab Application Note EC08, *"Basic overview of the working principle of a potentiostat/galvanostat (PGSTAT)-Electromechanical cell setup"*, Available: http://www.ecochemie.nl/download/Applicationnotes/Autolab_Application_Note_EC08.pdf

[30] Nicolá Pérez, Flávio Buiochi, Marco Aurélio Brizzotti Andrade and Julio Cezar Adamowski, *"Numerical Characterization of Piezoceramics Using Resonance Curves"*, 2016, Materials (Volume: 9, Issue: 2), Available: http://dx.doi.org/10.3390/ma9020071

[31] J. A. Nelder and R. Mead, *"A simplex method for function minimization"*, 1965, The Computer Journal (Volume: 7, Issue: 4, Pages: 308-313) Available: http://dx.doi.org/10.1093/comjnl/7.4.308

[32] David Charnegie, *Frequency tuning concepts for piezoelectric cantilever beams and plates for energy harvesting*, 2007

[33] http://www.daycounter.com/LabBook/Moving-Average.phtml

[34] Nicola Femia, Giovanni Petrone, Giovanni Spagnuolo, Massimo Vitelli, *"Power Electronics and Control Techniques for Maximum Energy Harvesting in Photovoltaic System"*, 2012, CRC Press (ISBN: 9781466506909), Available: https://www.crcpress.com/Power-Electronics-and-Control-Techniques-for-Maximum-Energy-Harvesting/Femia-Petrone-Spagnuolo-Vitelli/p/book/9781466506909

[35] Mickaël Lallart, Steven R. Anton and Daniel J. Inman, *"Frequency Self-tuning Scheme for Broadband Vibration Energy Harvesting"*, 2010, Journal of Intelligent Material System and Structures (Vol. 21, no. 9, Pages: 897-906), Available: http://dx.doi.org/10.1177/1045389X10369716

[36] Qing-Ming Wang, Xiao-hong Du, Baomin Xu and L. Eric Cross, *"Theoretical Analysis of the Effect of Cantilever Benders"*, 1999, Journal of applied physics (Vol. 85 no. 3), Available: http://dx.doi.org/10.1063/1.369314